Simultaneous Binding of Basic Peptides at Intracellular Sites on a Large Conductance Ca^{2+}-activated K^+ Channel

Equilibrium and Kinetic Basis of Negatively Coupled Ligand Interactions

ISABELLE FAVRE* and EDWARD MOCZYDLOWSKI*‡

From the *Department of Pharmacology and ‡Department of Cellular and Molecular Physiology, Yale University School of Medicine, New Haven, Connecticut 06520-8066

ABSTRACT The homologous Kunitz inhibitor proteins, bovine pancreatic trypsin inhibitor (BPTI) and dendrotoxin I (DTX-I), interact with large conductance Ca^{2+}-activated K^+ channels (maxi-K_{Ca}) by binding to an intracellular site outside of the pore to produce discrete substate events. In contrast, certain homologues of the *Shaker* ball peptide produce discrete blocking events by binding within the ion conduction pathway. In this study, we investigated ligand interactions of these positively charged peptide molecules by analysis of single maxi-K_{Ca} channels in planar bilayers recorded in the presence of DTX-I and BPTI, or DTX-I and a high-affinity homologue of ball peptide. Both DTX-I (K_d, 16.5 nM) and BPTI (K_d, 1,490 nM) exhibit one-site binding kinetics when studied alone; however, records in the presence of DTX-I plus BPTI demonstrate simultaneous binding of these two molecules. The affinity of BPTI (net charge, +6) decreases by 11.7-fold (K_d, 17,500 nM) when DTX-I (net charge, +10) is bound and, conversely, the affinity of DTX-I decreases by 10.8-fold (K_d, 178 nM) when BPTI is bound. The ball peptide homologue (BP; net charge, +6) exhibits high blocking affinity (K_d, 7.2 nM) at a single site when studied alone, but has 8.0-fold lower affinity (K_d, 57 nM) for blocking the DTX-occupied channel. The affinity of DTX-I likewise decreases by 8.4-fold (K_d, 139 nM) when BP is bound. These results identify two types of negatively coupled ligand–ligand interactions at distinct sites on the intracellular surface of maxi-K_{Ca} channels. Such antagonistic ligand interactions explain how the binding of BPTI or DTX-I to four potentially available sites on a tetrameric channel protein can exhibit apparent one-site kinetics. We hypothesize that negatively coupled binding equilibria and asymmetric changes in transition state energies for the interaction between DTX-I and BP originate from repulsive electrostatic interactions between positively charged peptide ligands on the channel surface. In contrast, there is no detectable binding interaction between DTX-I on the inside and tetraethylammonium or charybdotoxin on the outside of the maxi-K_{Ca} channel.

KEY WORDS: aprotinin • bovine pancreatic trypsin inhibitor • charybdotoxin • dendrotoxin • Kunitz inhibitor

INTRODUCTION

Large conductance (~250 pS) Ca^{2+}-activated K^+ channels (BK or maxi-K_{Ca} channels)[1] are an intriguing class of ion channels that are activated in a synergistic fashion by intracellular Ca^{2+} and depolarizing voltage (Latorre, 1994). In *Drosophila*, maxi-K_{Ca} channels are encoded by the *Slowpoke* gene, part of which is homologous to the family of voltage-gated K^+ channels (K_V channels), including *Shaker* (Atkinson et al., 1991; Adelman et al., 1992). Both K_V and *Slowpoke* channels contain a characteristic motif of six membrane-spanning segments called S1–S6. This motif includes the S4 segment involved in voltage sensing and the extracellular P-region between S5 and S6 that determines ionic selectivity. Besides these common structural elements, *Slowpoke* maxi-K_{Ca} channels have an additional transmembrane segment at the NH_2 terminus, called S0, plus a unique sequence of ~800 residues at the COOH terminus (Meera et al., 1997). Substantial evidence supports the notion that the COOH-terminal portion of the maxi-K_{Ca} channel protein corresponds to a large cytoplasmic domain that contains Ca^{2+}-binding site(s) involved in channel activation (Wei et al., 1994; Schreiber and Salkoff, 1997). To understand the mechanism of Ca^{2+} activation and biochemical regulation of maxi-K_{Ca} channels, it is necessary to define the structure and function of this cytoplasmic domain. An underlying objective of the work described in this paper is to characterize intracellular binding sites for peptide

Address correspondence to Dr. Edward Moczydlowski, Department of Pharmacology, Yale University School of Medicine, Sterling Hall of Medicine, P.O. Box 208066, New Haven, CT 06520-8066. Fax: 203-785-7670; E-mail: Edward_Moczydlowski@yale.edu

[1]*Abbreviations used in this paper:* BP, *Shaker* ball peptide homolog; BPTI, bovine pancreatic trypsin inhibitor; ChTX, charybdotoxin; DTX-I, Toxin I of *Dendroaspis polylepis*; maxi-K_{Ca}, large conductance Ca-activated K^+ channel; TEA, tetraethylammonium.

ligands that can serve as reference points in studies of the cytoplasmic architecture of the maxi-K_{Ca} channel.

The charybdotoxin family of small protein toxins is a set of natural ligands that has been effectively used to identify structural determinants in the extracellular pore region of K^+ channels (Miller, 1995; MacKinnon et al., 1998). By analogy, protein ligands that bind to intracellular sites on maxi-K_{Ca} channels may similarly be useful for mapping this part of the channel protein. One class of such ligands is the Kunitz family of proteins that includes bovine pancreatic trypsin inhibitor (BPTI) and dendrotoxin-I (DTX-I). This family of ~60-residue proteins shares six conserved Cys residues (see Fig. 1 A) and a common protein fold, but its members exhibit diverse inhibitory activities. BPTI and related Kunitz molecules are potent inhibitors of various members of the chymotrypsin/trypsin family of serine proteinases (Dufton, 1985; Capasso et al., 1997). DTX-I and several homologues from mamba snake venom block various K_V channels from the extracellular side, but are poor inhibitors of serine proteinases (Hollecker et al., 1993; Smith et al., 1997). Calcicludine, another Kunitz homologue from mamba venom, blocks high-threshold voltage-activated Ca^{2+} channels from the extracellular side (Schweitz et al., 1994). Yet another activity exhibited by some Kunitz proteins such as DTX-I and BPTI is a rather distinctive inhibitory effect on maxi-K_{Ca} channels from the intracellular side (Lucchesi and Moczydlowski, 1990, 1991). This latter effect resembles a slow blocking reaction, but differs in that the individual blocking events mimic subconductance states at the single-channel level. Apparent subconductance events induced by BPTI and DTX-I are actually due to a fast closing and opening reaction of the maxi-K_{Ca} channel in the ligand-bound state (Moss and Moczydlowski, 1996). For descriptive purposes, this behavior is referred to here simply as "substate behavior" or "substate events." In contrast to the substate-inducing behavior of Kunitz inhibitors, an NH_2-terminal inactivation domain of *Shaker* K_V channels called the "ball peptide" is known to directly block maxi-K_{Ca} channels by binding within the internal vestibule or pore (Foster et al., 1992; Toro et al., 1992).

To further develop Kunitz inhibitors as structural probes of the intracellular domain of maxi-K_{Ca} channels, it is necessary to localize the binding site of these inhibitors with respect to the primary sequence of the channel. One line of evidence that such ligands do not occlude or bind directly in the pore is that the blocking affinity of internal Ba^{2+} and internal tetraethylammonium (TEA) is not significantly affected by BPTI and DTX-I, respectively (Lucchesi and Moczydlowski, 1991). Such results lead to the hypothesis that BPTI and DTX-I bind to an intracellular site outside the pore and induce substate behavior by an allosteric mechanism. A potential candidate for the BPTI/DTX-I binding site on the K_{Ca} channel protein is a region of ~250 residues near the COOH terminus that exhibits similarity to the chymotrypsin family of serine proteinases (Moss et al., 1996a,b). However, serious consideration of this hypothesis leads to an interesting paradox. Since maxi-K_{Ca} channels are probably formed as homotetramers of four identical α-subunits (Shen et al., 1994), how can BPTI and DTX-I bind outside the central pore or common fourfold subunit interface and yet exhibit binding kinetics characteristic of a single site? The allosteric model of substate production invoked above predicts that four binding sites for BPTI/DTX-I must exist on each tetrameric channel complex. Such a model further predicts that the kinetics of BPTI/DTX-I association and dissociation ought to reflect multiple sites of ligand interaction.

To resolve this question, we investigated the interaction of BPTI and DTX-I with rat muscle K_{Ca} channels inserted into planar lipid bilayers. The titration behavior of single K_{Ca} channels with BPTI in the presence of DTX-I deviated significantly from simple binding competition of two ligands at a single site. The data are consistent with a model that includes states of simultaneous occupancy by one BPTI and one DTX-I molecule on different subunits of a tetrameric complex. Binding of DTX-I to one subunit lowers the binding affinity for BPTI on another subunit by ~11-fold, and vice versa. To further probe the location of the Kunitz inhibitor site with respect to the pore, we analyzed the single-channel blocking kinetics of a homologue of *Shaker* ball peptide (BP) in the absence and presence of DTX-I. The results indicate that BP binds to the K_{Ca} channel with an approximately eightfold lower affinity when DTX-I is simultaneously bound. Detailed analysis revealed that the lower affinity for BP is solely due to a 44-fold reduction in its association rate. Unexpectedly, we found that DTX-I actually stabilizes BP on its binding site by slowing its rate of dissociation by a factor of ~5.6. Overall, these results provide direct evidence of negatively coupled ligand–ligand interactions among sites for Kunitz proteins and ball peptide that take place on the intracellular surface of maxi-K_{Ca} channels. The unusual asymmetry of energetic effects on rate constants for the interaction between DTX-I and BP can be explained by structural features inherent to a channel-like architecture.

MATERIALS AND METHODS

Planar Bilayer Recording

Planar bilayers were formed on a 0.2-mm diameter hole drilled in a cylindrical cup made of polystyrene or delrin as supplied by Warner Instrument Corp. The membrane was cast from a solution of 25 mg/ml phospholipids in decane. Bilayer formation was mon-

itored by capacitance measurement. The lipid composition was a mixture of 80% 1-palmitoyl-2-oleoyl-sn-glycero-3-phosphoethanolamine and 20% 1-palmitoyl-2-oleoyl-sn-glycero-3-phosphocholine (Avanti Polar Lipids). Plasma membrane vesicles were prepared from adult rat skeletal muscle using the procedure described in Favre et al. (1999). The final recording solution on both sides of the bilayer contained 50 mM KCl, 10 mM MOPS-KOH, pH 7.4. Incorporation of maxi-K_{Ca} channels from membrane vesicles into planar bilayers followed methods described previously (Lucchesi and Moczydlowski, 1991). Only bilayers containing single maxi-K_{Ca} channels were used for these experiments. The intracellular or internal side of the bilayer is defined as the side that responds to activation of K_{Ca} channels by Ca^{2+} and positive voltage. For all experiments in this work, the holding voltage was +30 mV using the physiological convention of extracellular ground. The internal Ca^{2+} concentration was usually 200 μM, but was increased to 500 μM in some experiments to maintain the open state probability of intrinsic K_{Ca} channel gating at >0.9.

Single channel currents were recorded at room temperature (20–23°C) using a patch clamp amplifier (3900A; Dagan Corp.) with an expander (3910; Dagan Corp.) for bilayer capacitance measurements. The patch clamp headstage was connected to the bilayer chamber via Ag/AgCl electrodes and agar-KCl bridges. Single channel recordings were stored on VCR tape using a digital data recorder (VR-10; Instrutech Corp.). Data were filtered at a corner frequency of 100–500 Hz with an eight-pole low pass Bessel filter (902LPF; Frequency Devices Inc.) and sampled at five times the filter frequency or greater for subsequent analysis.

Bovine pancreatic trypsin inhibitor was purchased from Sigma Chemical Co. Dendrotoxin I (or toxin I from *Dendroaspis polylepis*) was obtained from Alomone Labs. A peptide homologue (BP) of the *Shaker* ball peptide with the primary sequence MAAVAVLYVLGKKRQHRKKQ was synthesized by the W.M. Keck Biotechnology Resource Center at Yale University Medical School (New Haven, CT). The purity of the peptide was confirmed by reverse phase HPLC and mass spectroscopy (mol wt, 2,325). Concentrated stock solutions of 500 μM BP were prepared in H_2O. Problems associated with adsorption of BP to the plastic chambers were minimized by adding vesicles and BP to the front chamber, composed of black delrin, rather than the rear cup chamber, composed of polystyrene. Peptide concentrations are based on dry weight and supplier information. Therefore, derived k_{on} and K_d values should be regarded as relative rather than absolute measurements.

Single Channel Analysis

These experiments involved long recordings (~1–5 h) of single maxi-K_{Ca} channels exposed to the following inhibitors: DTX-I, BPTI, BP, TEA, and charybdotoxin (ChTX). After addition of a particular concentration of an inhibitor that induced discrete events, channel activity was continuously recorded for a time sufficient to collect ~100 events when possible. Then, the next concentration of inhibitor was added, channel activity was recorded, etc., until the bilayer broke. Substate events induced by DTX-I (mean dwell time ~38 s) were the longest events that were measured and analyzed. Durations of these latter events were measured directly from chart records with the aid of a digitizing tablet (TG1017; Houston Instrument). Substate events induced by BPTI (mean dwell time ≃ 0.41 s) and BP blocking events (mean dwell time ≃ 1.7 s) were automatically measured from digitized records using an LSI 1173 computer system (Indec). For this purpose, single-channel data was filtered at 100 Hz and sampled at 1 kHz. Transitions were detected using a 50% threshold criterion set between the substate current level and the open state for BPTI or between the zero current (blocked state) and open state for BP. To exclude brief closures due to intrinsic channel gating, a cutoff limit of $\alpha = 0.1$ s was used for the shortest acceptable substate closure or blocked state event. This cutoff limit excludes >95% of Ca^{2+}- and voltage-dependent closures due to channel gating under these conditions (200 μM internal Ca^{2+} and +30 mV).

Lifetimes of BPTI-substate, BP-blocked, ChTX-blocked, or unblocked state events were generally measured from populations of dwell times ($n > 100$ events) that were binned, plotted as cumulative probability distributions, and fit to an exponential function of time. These distributions were invariably well described by a single exponential (Lucchesi and Moczydlowski, 1991). Measured lifetimes of the unoccupied open state or unblocked state were corrected for a small amount of artificial lengthening due to the minimum cutoff limit for closures of $\alpha = 0.1$ s using the following formula (Colquhoun and Sigworth, 1983): $\tau_{corrected} = \tau_{observed} \exp(-\alpha/\tau_{closed})$. Certain types of event samples such as DTX-I substates, burst lengths, or BP-blocked events in the presence of DTX-I were measured as simple arithmetical means. Arithmetical means were used in these latter cases, either because the sample size was often <100 events and not well suited to histogram fitting, or because the analysis focused on the behavior of the actual mean dwell time of more complex distributions (e.g., see Eq. 19). Dwell-time histograms obtained in the presence of DTX-I and BP exhibited two exponential components. These data were also plotted as probability density functions and fit to a sum of two exponentials using PCLAMP analysis software from Axon Instruments.

Single-channel block by external TEA was manifested as a "fast block" corresponding to an apparent decrease in unitary current (e.g., Moczydlowski, 1992). Unitary current as a function of [TEA] was measured with the use of all-points amplitude histograms to determine the mean value of the closed and apparent open state current levels. Kinetic parameters directly measured from single-channel data are reported as the mean ± SD or SEM ($SEM = SD/\sqrt{n}$), as noted in the text. Estimates of propagated errors for parameters calculated from kinetic equations are based on standard rules for the additivity of variance (i.e., absolute variance is additive for addition and subtraction; relative variance is additive for multiplication and division). Nonlinear curve fitting to various equations was carried out using SigmaPlot software (SPSS Inc.) based on the Marquardt-Levenberg algorithm.

RESULTS

Kinetics of BPTI-induced Substate Events Are Well Described by a One-Site Process

Previous studies of DTX-I– and BPTI-induced substate events suggested that these ligands bind reversibly to a single intracellular site or homogeneous class of sites on maxi-K_{Ca} channels that is located outside the pore (Lucchesi and Moczydlowski, 1990, 1991). However, this conclusion appears to be in conflict with the known tetrameric structure of K^+ channels and the prevailing idea that the functional unit of maxi-K_{Ca} channels is a tetramer of ~130 kD α-subunits (Shen et al., 1994; Doyle et al., 1998). A nonpore binding site on a homotetrameric channel structure implies that there should be four symmetrically located sites on the cytoplasmic side of the protein. To pursue this question, we re-examined the kinetics of BPTI-induced substate

events as a function of BPTI concentration to ascertain whether one-site behavior is strictly obeyed.

Fig. 1 B shows typical results from an experiment in which a single K_{Ca} channel recorded at a high open-state probability is consecutively exposed to 1, 2, 4, and 8 μM internal BPTI. These records show that BPTI induces a noisy but well-defined substate at ~27% of the unitary current and that the channel's probability of residing in this substate increases with BPTI concentration. The records also show a few examples of well resolved closures to the zero current level, plus other subconductance levels that are occasionally observed under these conditions. However, these latter events are quite rare compared with the time the channel spends in the open state and the major substate. They are ignored for this analysis since they occur too infrequently for quantitative evaluation.

A possible model for binding of BPTI to four equivalent sites on a homotetramer is shown in Fig. 2, Scheme 1. For the sake of discussion, this model assumes that the microscopic association rate constants, k_1, for binding to a site on each of the four subunits of the unliganded U state are equivalent. With this assumption, the observed macroscopic association rate constant for binding of one BPTI molecule to the U state would be $4k_1$. Similar statistical factors apply to the other association and dissociation steps involving binding to or unbinding from multiply occupied states. Fig. 2, Scheme 1, is only one possible example of a sequential reaction that could describe ligand binding to a homotetrameric protein. Many other ligand binding schemes are possible, including mechanisms that involve conformational changes of individual subunits or the whole complex. The essential point is that ligand binding to multisubunit complexes can potentially display complex behavior including positive and negative cooperativity.

If more than one BPTI molecule can bind to a single tetrameric K_{Ca} channel complex, one would expect to observe some indication of the existence of more than one class of ligand-bound states in single channel records. In the experiment of Fig. 1 B, increasing BPTI concentration from 0 to 8 μM decreases the probability of the channel residing in the fully open conductance state from 1.0 to ~0.15. However, evidence for different states of BPTI occupancy (e.g., states S_1–S_4 of Fig. 2, Scheme 1) is not obvious from the single-channel record. One ex-

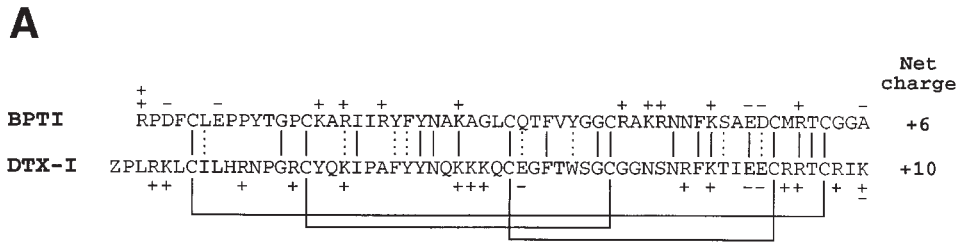

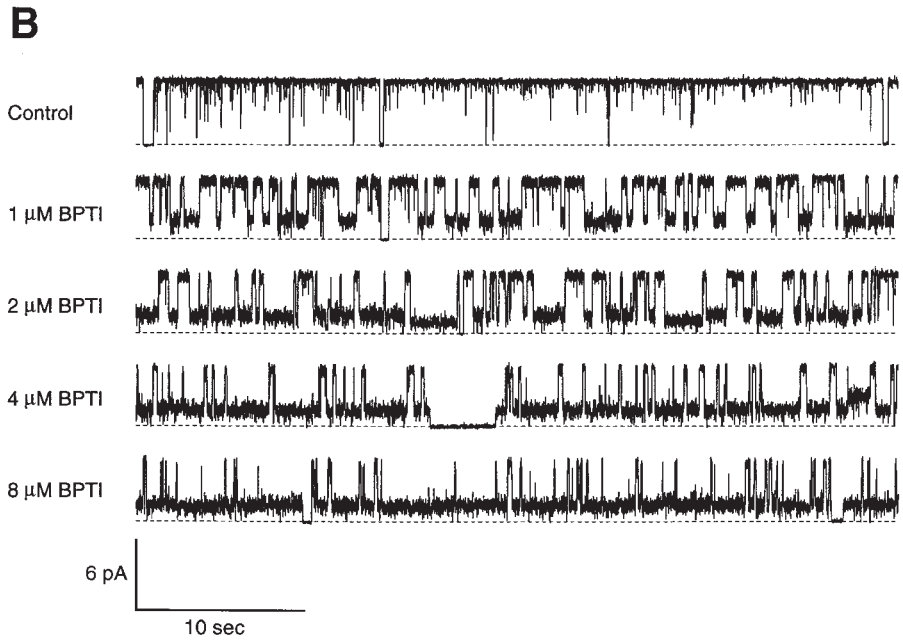

FIGURE 1. Titration of a single K_{Ca} channel with BPTI. (A) Comparison of the primary sequence of BPTI and DTX-I using the one letter amino acid code (Z, pyroglutamate). A short solid line marks two identical residues and a dotted line indicates chemical similarity. Connecting lines denote three disulfide bonds in both molecules. (B) Representative current records from a single rat muscle K_{Ca} channel recorded under control conditions (symmetrical 50 mM KCl, 10 mM MOPS-KOH, pH 7.4, 200 μM internal $CaCl_2$) and after addition of 1, 2, 4, and 8 μM internal BPTI. The holding voltage in this and all other experiments is +30 mV. The dashed line identifies the zero-current level.

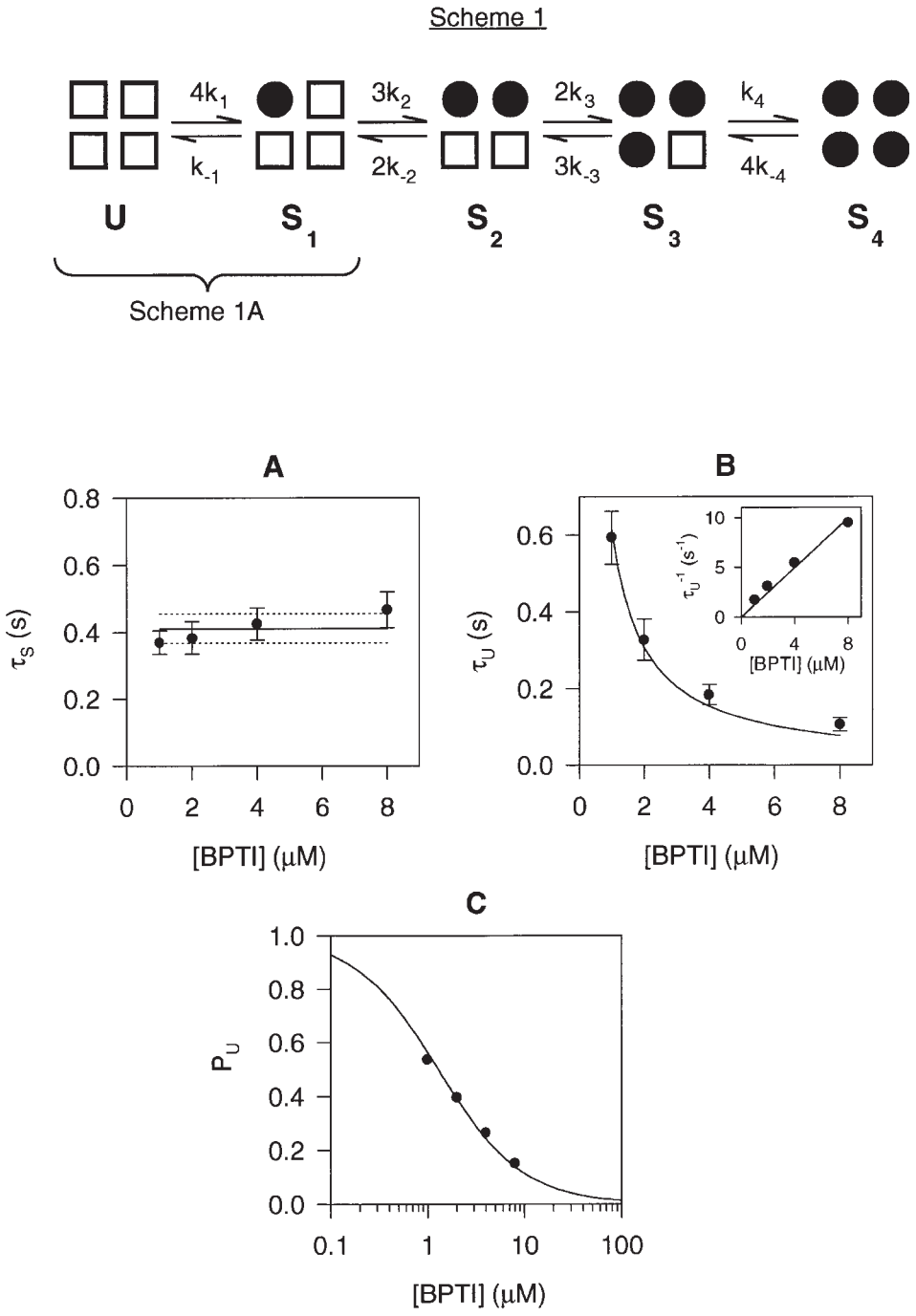

FIGURE 2. Kinetic analysis of BPTI substate events. Scheme 1 is a hypothetical five-state model for binding of a ligand such as BPTI to four equivalent sites on a homotetrameric K_{Ca} channel. □, unoccupied subunits; ●, BPTI-occupied subunits. Upper rate constants, k_1, k_2, k_3, and k_4, are bimolecular association rate constants; lower rate constants, k_{-1}, k_{-2}, k_{-3}, and k_{-4}, are first order dissociation rate constants. Integers preceding the rate constants are statistical factors. (A) Lifetime of BPTI-substate events as a function of [BPTI]. (B) Lifetime of dwell times between adjacent BPTI-substate events as a function of [BPTI]. Data points and error bars in A and B are the mean ± SEM for seven to eight single channels. The solid line and two dotted lines in A are the mean ± SD of four data points used to measure k_{-1} from the lifetime τ_S of substate S1 (Eq. 1). The solid line in B is a fit to Eq. 2 used to measure $4k_1$ from the lifetime τ_U of state U (Eq. 2). The inset shows the same data plotted as the reciprocal lifetime. (C) Time-averaged probability of a channel being in the unoccupied (BPTI-free) state as a function of [BPTI]. Each point was calculated from 6.3–6.9 h of data pooled from seven or eight single channels. The solid line in C is a fit to $P_U = K_1/(K_1 + [\text{BPTI}])$ used to measure the equilibrium constant K_1 as described in the text.

planation may be that the binding of one, two, three, or four BPTI molecules produces a channel with exactly the same conductance behavior, corresponding to the ~27% substate level. However, if this were the case, the probability distribution for the dwell time in the substate would correspond to the distribution of a group of four states, S1, S2, S3, and S4, within the framework of Fig. 2, Scheme 1. The predicted theoretical form for this distribution would be a sum of four exponential components. Furthermore, Fig. 2, Scheme 1 predicts that the distribution of substate dwell times would be dependent on BPTI concentration. Thus, the mean substate dwell time should lengthen with BPTI concentration if Fig. 2, Scheme 1 is applicable.

To search for such behavior, dwell time histograms of BPTI-substate events were compiled for eight different single channels at 1, 2, 4, and 8 μM BPTI, as described in MATERIALS AND METHODS. Consistent with previous work (Lucchesi and Moczydlowski, 1991), these histograms conformed to a single exponential distribution

at all BPTI concentrations (not shown). The mean lifetime of the exponentially distributed BPTI substate (τ_s) was equal to 0.411 ± 0.022 s (Fig. 2 A). Although there is a slight tendency for τ_s to increase with [BPTI] in Fig. 2 A, the data points at 1, 2, 4, and 8 μM BPTI are not statistically different by the usual criterion of $P \leq 0.05$. Thus, there is no hard evidence that the mean duration of the BPTI-induced substate lengthens significantly with increasing [BPTI] or that there is a kinetically distinct population containing >5% of the total substate events. These results confirm that the kinetics of BPTI-induced substate events are well described by a one-site process such as that represented by Fig. 2, Scheme 1A.

Fig. 2, Scheme 1A, predicts the following relationships for the lifetime, τ_S, of the S1 BPTI substate, and for the lifetime, τ_U, of the unliganded U state:

$$\tau_S = (k_{-1})^{-1} \quad (1)$$

$$\tau_U = (4k_1[\text{BPTI}])^{-1}. \quad (2)$$

The dissociation rate constant, k_{-1}, calculated according to Eq. 1 from the reciprocal of the mean of four τ_S measurements in Fig. 2 A is $k_{-1} = 2.43 \pm 0.13\ s^{-1}$ (±SEM). The observed association rate constant, $4k_1$, can be obtained from the reciprocal relationship between τ_U and [BPTI] according to Eq. 2. Probability histograms of unliganded U-state events between adjacent BPTI substates were also uniformly well described by a single exponential function (not shown). The mean lifetime of τ_U measured for eight different single channels at each BPTI concentration is plotted in Fig. 2 B and fit to Eq. 2. This fit gives an estimate of $4k_1 = 1.63 \pm 0.07 \times 10^6\ s^{-1}M^{-1}$ for the apparent BPTI-association rate constant. The kinetic ratio, $k_{-1}/4k_1$, or $K_1 = 1.49 \pm 0.10$ μM, is the equilibrium dissociation constant for BPTI in Fig. 2, Scheme 1A.

The K_1 equilibrium constant can also be estimated from the time-averaged probability of the unliganded state, P_U. Fig. 2, Scheme 1A, predicts that $P_U = K_1/(K_1 + [\text{BPTI}])$. A fit of the data in Fig. 2 C to this latter function yields $K_1 = 1.28 \pm 0.07$ μM, in agreement with the kinetic ratio of $k_{-1}/4k_1$. For models such as Fig. 2, Scheme 1, where there is a substantial population of multi-liganded states, Hill coefficients (n) higher than $n = 1$ are also predicted. The fact that the data of Fig. 2 C is closely fit using an n of 1.0 is additional evidence that Fig. 2, Scheme 1A, or an equivalent one-site model describes the interaction of BPTI with the maxi-K_{Ca} channel. Thus, if the K_{Ca} channel does contain four structurally homologous BPTI binding sites in the tetrameric complex, the kinetic data imply that the binding of BPTI to one of the sites essentially precludes the binding of a second BPTI molecule to any of the remaining three sites.

Complex Behavior of BPTI Burst Durations in the Presence of DTX-I Is Evidence for Simultaneous Occupancy by BPTI and DTX-I

The sequence alignment of Fig. 1 A illustrates that BPTI (58 residues) and DTX-I (60 residues) are 32% identical, including the presence of six conserved Cys residues. It is also known that these two small proteins share a common fold at the tertiary structural level (Berndt et al., 1993; Lancelin et al., 1994; Skarzynski, 1992). Like BPTI, DTX-I also induces discrete substate events when added to the intracellular side of maxi-K_{Ca}

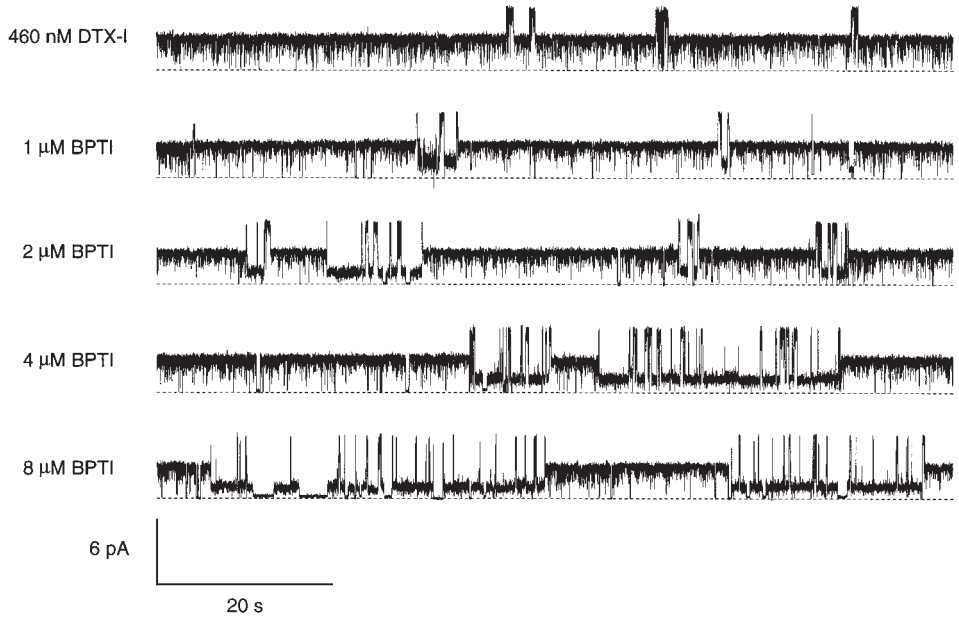

FIGURE 3. Representative segments of current records from a single K_{Ca} channel recorded in the presence of DTX-I and increasing concentrations of BPTI. (A) A single rat muscle K_{Ca} channel was recorded under control conditions described in Fig. 1. DTX-I (460 nM) was added to the internal side followed by 1, 2, 4, and 8 μM internal BPTI, as indicated. The dotted line marks the zero current level.

channels, but the average duration of the DTX-I–induced substate is ~38 s compared with ~0.41 s for BPTI. Fig. 3 (top) shows a segment of a typical single-channel recording taken after addition of 460 nM DTX-I. Long-lived substate events induced by DTX-I typically exhibit less excess noise and a higher mean current level (~60% of unitary current at +30 mV) than the shorter duration BPTI substate (Fig. 1 B). Previous studies have also established that the kinetics of interaction of DTX-I with single K_{Ca} channels is well described by a one-site process equivalent to Fig. 2, Scheme 1A, discussed above for BPTI (Lucchesi and Moczydlowski, 1990, 1991). To investigate the physical relationship of binding sites for BPTI and DTX-I, we examined the effect of titrating single maxi-K_{Ca} channels with increasing concentrations of BPTI in the presence of a nearly saturating concentration of DTX-I.

In the presence of 460 nM DTX-I alone (Fig. 3, top), single K_{Ca} channels exhibit two distinct states or modes of activity: (a) long-lived substates at ~60% of the unitary current that correspond to residence times of DTX-I on the channel, and (b) shorter intervals between adjacent DTX-substates defined as "inter-DTX periods." The latter periods correspond to waiting times of the unoccupied channel between the dissociation of one DTX-I molecule and association of another. If BPTI can bind to a channel that is already occupied by DTX-I, one might expect to observe discrete interruption of the long-lived DTX substate with short BPTI-like substate events. Alternatively, if binding of BPTI to the unoccupied channel is greatly favored over binding to the DTX-occupied channel, then brief BPTI-substates should occur only within inter-DTX periods.

The data of Fig. 3 illustrate that the system is best described by the latter alternative. Long recordings from such experiments reveal that titration of BPTI in the presence of DTX-I exhibits a pattern of activity that may be roughly described as bursts of BPTI-substate activity punctuated by DTX substates. In particular, records of Fig. 3 obtained in the presence of both ligands show that two adjacent DTX-substate events are nearly always flanked on both the exit and entry side by transitions to the fully open current level. This implies that DTX-I usually dissociates before a burst of shorter BTPI-binding events begins and that BPTI usually dissociates before DTX-I can bind to produce a long-lived substate. To quantitate this latter observation, 458 inter-DTX periods were examined for the type of first transition flanking the exit from the DTX-substate current level and the entry back to the next DTX substate. This analysis revealed that 96.1% of all DTX substates were terminated by an opening to the fully open current level and 95.6% of all inter-DTX periods were terminated by a transition from the fully open current level to the DTX-substate level. These measurements confirm the visual impression from the single-channel records that DTX-I preferentially dissociates before BPTI can bind to the channel, and vice versa.

Such behavior is expected for a mechanism like that shown in Fig. 4, Scheme 2A. This model is an extension of Fig. 2, Scheme 1A, for formation of the BPTI substate (S_{BPTI}) that includes binding of DTX-I to the unoccupied channel (U) to produce the DTX substate (S_{DTX}). The implicit assumption of Fig. 4, Scheme 2A, is that, by virtue of structural homology, BPTI and DTX-I bind to the same site(s) on a K_{Ca} channel tetramer, but that some mechanism strongly inhibits binding of more than one of these molecules at a time. Although there are four potentially available sites on the tetrameric complex, Fig. 4, Scheme 2A, is formally equivalent to simple, mutually exclusive competition of two ligands at a single site and may be referred to as "pseudo one-site competition."

The cursory description of data from experiments of Fig. 3 outlined so far generally supports Fig. 4, Scheme 2A. However, there are indications that the system is actually more complex. Particularly at higher concentrations of BPTI, current records of Fig. 3 (8 μM BPTI) display a new type of event. Many of the inter-DTX periods exhibit one or more states of very low conductance or "nearly blocked" events that last several seconds in duration. These latter events begin with a decrease in current from the BPTI-substate level to a level near zero current and terminate with an increase in current directly back to the BPTI-substate level. Such events are quite rare in the presence of BPTI alone (Fig. 1 B), but they are noticeably more frequent in the presence of DTX-I. These latter observations lead to the hypothesis that the BPTI substate is susceptible to conversion to a different type of low-conductance state in the presence of DTX-I. With BPTI alone, doubly bound states (Fig. 2, Scheme 1, S2) may occur with very low probability such that their contribution to the time-averaged behavior is hard to rigorously detect (e.g., on the order of 1% or less). However, in the presence of DTX-I plus BPTI, a state in which both ligands are bound simultaneously may occur with a probability that is high enough to measure a significant deviation from purely one-site behavior.

To pursue this latter conjecture, we analyzed whether the detailed kinetic behavior obeys the strict predictions of Fig. 4, Scheme 2A. The first step in this analysis requires determination of the dissociation and apparent association rate constants (j_{-1}, $4j_1$, respectively) for DTX-I in the absence of BPTI from relationships analogous to those of Eqs. 1 and 2:

$$\tau_{S-DTX} = (j_{-1})^{-1} \quad (3)$$

$$\tau_{U} = (4j_1[DTX])^{-1}. \quad (4)$$

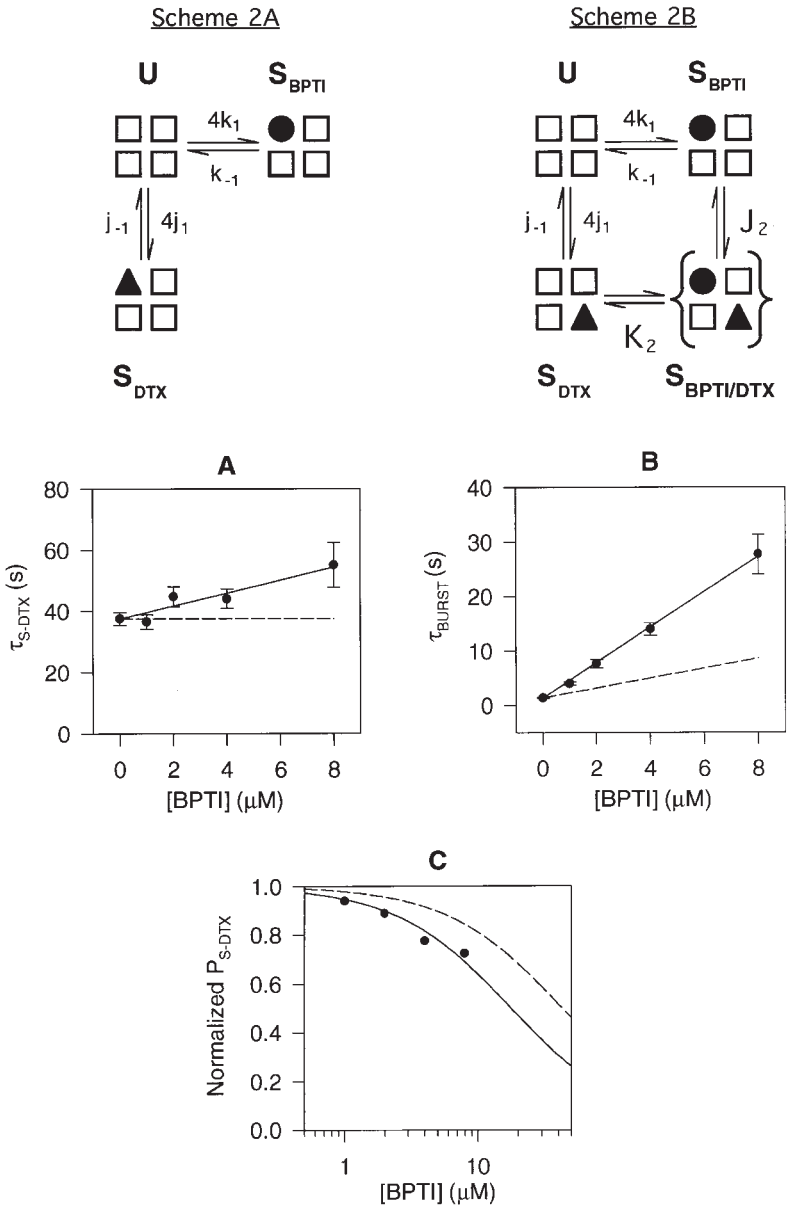

FIGURE 4. Kinetic analysis of ligand interactions between DTX-I and BPTI. Scheme 2A shows a three-state model for simple binding competition between two different Kunitz inhibitor ligands. The model assumes that only one BPTI or DTX-I molecule can bind on a K_{Ca} channel homotetramer at any given time and that equivalent rates are observed for each of the four subunits. □, unoccupied subunits; ●, a BPTI-bound subunit; and ▲, a DTX-I–bound subunit. Scheme 2B shows a more complex four-state model that allows for the possibility that one BPTI molecule and one DTX-I molecule can bind simultaneously on two different subunits. (A) Lifetime of the apparent DTX-I substate as a function of BPTI concentration. Events identified as apparent DTX-I substates were pooled from 5–18 single channels for each condition. Each data point represents the mean ± SEM for samples of 71–358 events. The dashed line is the behavior expected for Scheme 2A according to Eq. 5. The solid line is a fit to Eq. 8 derived for Scheme 2B. (B) Lifetime, as a function of [BPTI], of the complex burst state defined as the interval between two consecutive DTX-I substates. The data pool and sample sizes used for calculating the mean ± SEM were the same as that for A. The dashed line is the behavior expected for Scheme 2A according to Eq. 6. The solid line is a fit to Eq. 7 derived for Scheme 2B. (C) Time-averaged probability of residing in the apparent DTX-I substate as a function of BPTI concentration. The measured probability of the DTX-I substate is normalized to that in the absence of BPTI ($P^0_{S\text{-}DTX} = 0.968$). The dashed line is the prediction for Scheme 2A according to Eqs. 10 and 11. The solid line is a fit to Eq. 10 using $K_{App} = 17.8$ μM.

The mean dwell time of the DTX substate, $\tau_{S\text{-}DTX}$, was measured as 37.6 ± 2.1 s (±SEM) from a population of 358 events pooled from 18 different single K_{Ca} channels. Likewise, the mean dwell time of the unoccupied channel measured in the presence of 460 nM DTX-I, τ_U, was 1.35 ± 0.09 s (±SEM). These values were used to calculate the rate constants, $j_{-1} = 0.0266 \pm 0.0015$ s^{-1} and $4j_1 = 1.61 \pm 0.11 \times 10^6$ $s^{-1}M^{-1}$ from Eqs. 3 and 4, respectively. The apparent equilibrium dissociation constant for DTX-I is obtained as follows: $J_1 = j_{-1}/4j_1 = 16.5 \pm 1.4$ nM.

For a system that strictly adheres to the pseudo one-site competition mechanism of Fig. 4, Scheme 2A, the dwell time of the apparent DTX substate is expected to be independent of BPTI concentration. In contrast, the dwell time between adjacent DTX substates is expected to increase with BPTI concentration, as the channel spends more time in the combined burst state of U and S_{BPTI}. These relationships can be derived from Fig. 4, Scheme 2A, as follows:

$$\tau_{S-DTX} = (j_{-1})^{-1} \tag{5}$$

$$\tau_{BURST} = (4j_1[DTX])^{-1}\left\{1 + \frac{[BPTI]}{K_1}\right\}. \tag{6}$$

Durations of the apparent DTX substate corresponding to the lifetime predicted by Eq. 5 and inter-DTX periods or BPTI "bursts" corresponding to the lifetime predicted by Eq. 6 can be readily identified and measured from current records of such experiments. Fig. 4 A shows a plot of the lifetime of the apparent DTX substate at 460 nM DTX-I as [BPTI] is varied over the

range of 0–8 μM. The dashed line in Fig. 4 A is the prediction of Scheme 2A as stated by Eq. 5. In contrast to predicted independence with respect to [BPTI], the data reveal a significant lengthening of $\tau_{S\text{-}DTX}$ with increasing BPTI concentration. In quantitative terms, there is a 47% increase in the mean value of $\tau_{S\text{-}DTX}$ over the range of 0–8 μM BPTI. The underlying basis for the increase in $\tau_{S\text{-}DTX}$ with increasing [BPTI] appears to be an increased frequency of discrete low conductance events of several seconds in duration that occasionally interrupt DTX substates (not shown). Fig. 4 B shows a plot of the measured lifetime of inter-DTX periods or BPTI bursts as a function of [BPTI]. The dashed line in Fig. 4 B is the prediction for the simple competition mechanism of Scheme 2A according to Eq. 6, using previous derived values for $4j_1$ and K_1. The results of Fig. 4 B reveal a large deviation from the mechanism of Scheme 2A since the slope of the line described by the data (3.25 s/μM) is 3.6-fold greater than the slope of the dashed line predicted from Eq. 6 (0.91 s/μM). Thus, although the current records from experiments of Fig. 3 exhibit the type of behavior that is qualitatively expected for the pseudo one-site model of Fig. 4, Scheme 2A, the results of Fig. 4, A and B, show that there is a significant quantitative discrepancy.

A possible model to explain this discrepancy is shown in Fig. 4, Scheme 2B. This scheme assumes that one DTX-I molecule can bind with a certain affinity (equilibrium dissociation constant, J_2) to an unoccupied site on a channel that is already occupied by one BPTI molecule on a different subunit. We hypothesize that these latter DTX-binding events result in a doubly occupied mixed state ($S_{BPTI/DTX}$) that functionally corresponds to the very low conductance or "nearly blocked" states within BPTI bursts that were noted above in the description of Fig. 3. Fig. 4, Scheme 2B, predicts additional lengthening of apparent BPTI bursts as compared with Scheme 2A due to the low conductance interruptions caused by $S_{BPTI/DTX}$ states. In accord with Fig. 4, Scheme 2B, we assume that BPTI burst events represent dwell times in the compound state consisting of U, S_{BPTI}, and $S_{BPTI/DTX}$. Such burst events are defined as beginning with the appearance of the U state after dissociation of DTX from the S_{DTX} state, followed by prolonged sojourn in the $U \leftrightarrow S_{BPTI} \leftrightarrow S_{BPTI/DTX}$ equilibria, and ending with a transition from the U state back to the S_{DTX} state. With this definition, the following relationship applies:

$$\tau_{BURST} = (4j_1[DTX])^{-1}\left[1 + \frac{[BPTI]}{K_1}\left(1 + \frac{[DTX]}{J_2}\right)\right]. \quad (7)$$

Eq. 7 still requires that τ_{BURST} is a linear function of [BPTI] as observed in Fig. 4 B; however, it predicts a larger slope due to the additional factor of $(1 + [DTX]/J_2)$. Within this interpretive framework, Eq. 7 can be used to calculate the J_2 equilibrium constant for DTX binding to the S_{BPTI} state from the slope of τ_{BURST} vs. [BPTI] in Fig. 4 B (slope = 3.25 s/μM) and the values of $4j_1$ and K_1 derived previously. This calculation yields a value of 178 ± 17 nM for J_2. This estimate for J_2 implies that DTX binds to a channel that is occupied by BPTI with an affinity (J_2 = 178 nM) that is 10.8-fold weaker than that for DTX binding to the unoccupied channel (J_1 = 16.5 nM).

Fig. 4, Scheme 2B, can also be used to explain the results of Fig. 4 A. If we define the apparent DTX substate as beginning with an entry to the S_{DTX} state from the U state, followed by a possible sojourn in the $S_{DTX} \leftrightarrow S_{BPTI/DTX}$ equilibria, and ending with a transition from the S_{DTX} state back to the U state, then the following relation gives the predicted lifetime of this apparent DTX substate:

$$\tau_{S-DTX} = (j_{-1})^{-1}\left(1 + \frac{[BPTI]}{K_2}\right). \quad (8)$$

Comparison of Eqs. 8 and 5 shows that the apparent DTX substate, defined for Fig. 4, Scheme 2B, to include closures to the mixed $S_{BPTI/DTX}$ state, is lengthened relative to the DTX substate of Scheme 2A by the K_2 equilibrium. A fit of the data of Fig. 4 A to Eq. 8 yields a value of K_2 = 17.5 ± 2.9 μM for K_2. This result implies that the affinity for BPTI binding to the DTX-occupied channel (K_2 = 17.5 μM) is 11.7-fold weaker than that for the unoccupied channel (K_1 = 1.49 μM).

Although Fig. 4, Scheme 2B, seems to explain aspects of the bursting behavior of the two-ligand system of DTX-I and BPTI, there are indications of even further complexity. Specifically, the behavior of the nearly blocked events, assumed to represent the doubly occupied $S_{BPTI/DTX}$ state, appears to depend on which ligand binds first. Careful inspection of many current records reveals that such blocked states virtually always end with a transition back to the BPTI substate if they first begin with a transition from the BPTI substate. Similarly, such nearly blocked states virtually always end with a transition back to the DTX substate if they first begin with a transition from the DTX substate. This implies that the last ligand that binds to the channel is always the first ligand to come off the channel. For a simple cyclic equilibrium such as Fig. 4, Scheme 2B, the allowable routes of leaving a state should not depend on how the state was entered. This suggests that there is more than one type of doubly liganded state, $S_{BPTI/STX}$, and that the system is far more complex than that represented by the four-state equilibrium of Fig. 4, Scheme 2B. Nevertheless, we can evaluate whether Fig. 4, Scheme 2B, approximates a cyclic equilibrium by checking whether the following relationship holds:

$$\frac{K_2}{K_1} = \frac{J_2}{J_1}. \quad (9)$$

Using the estimated values for K_1, K_2, J_1, and J_2 obtained above, the ratio of the left side of Eq. 9 is 17.5/1.49 μM = 11.7 ± 2.1, and the ratio of the right side of Eq. 9 is 178/16.5 nM = 10.8 ± 1.4. The fact that these ratios are equivalent within the propagated error of our measurements supports the hypothesis that a coupled ligand interaction like that of Fig. 4, Scheme 2B, underlies the deviation from the pseudo one-site competition model of Scheme 2A.

Another parameter that is easily measured is the time-averaged probability of residing in the DTX substate, $P_{\text{S-DTX}}$. This probability was computed by dividing the sum of the durations of all recognized DTX substates at the 60% current level by the total time of the records. This measurement was made for data pooled from 6–18 single K_{Ca} channels for experiments of Fig. 3 at each tested concentration of BPTI. The resulting probability was normalized to obtain the probability ratio, $P_{\text{S-DTX}}/P^0_{\text{S-DTX}}$, by dividing $P_{\text{S-DTX}}$ by the probability of the DTX substate measured at 460 nM DTX in the absence of BPTI, $P^0_{\text{S-DTX}}$. The theoretical dependence on [BPTI] of this latter normalized probability can be derived for Fig. 4, Schemes 2A and 2B, as follows:

$$\frac{P_{\text{S-DTX}}}{P^0_{\text{S-DTX}}} = \frac{K_{\text{App}}}{K_{\text{App}} + [\text{BPTI}]} \tag{10}$$

$$K_{\text{App}} = K_1\left(1 + \frac{[\text{DTX}]}{J_1}\right) \tag{11}$$

$$K_{\text{App}} = K_1\left(\frac{1 + \frac{[DTX]}{J_1}}{1 + \frac{[DTX]}{J_2}}\right). \tag{12}$$

Both Schemes 2A and 2B of Fig. 4 predict an apparent "relief" of the normalized probability of the DTX substate with increasing [BPTI] that follows a titration curve given by Eq. 10. The parameter, K_{App}, of Eq. 10 is an apparent equilibrium constant that is given by Eq. 11 for Fig. 4, Scheme 2A, and Eq. 12 for Scheme 2B. The data points in Fig. 4 C are the values of the normalized probability ($P_{\text{S-DTX}}/P^0_{\text{S-DTX}}$) of the DTX substate measured in our experiments at 1, 2, 4, and 8 μM BPTI. The data shows that there is ~30% relief of the DTX substate at 8 μM BPTI. The theoretical curve, shown as a dashed line in Fig. 4 C, was calculated from Eqs. 10 and 11, where the K_{App} = 43.0 μM for Fig. 4, Scheme 2A, using the known values of K_1, J_1, and [DTX]. The fact that the measured data points clearly lie to the left of this curve with a significantly lower value for K_{App} is an independent piece of evidence that the system does not strictly obey the model of Scheme 2A. A nonlinear fit of the data in Fig. 4 C to Eq. 10 gives a best-fit value of K_{App} = 17.8 ± 1.7 μM. This latter estimate for K_{App} is close to the value of K_{App} = 12 ± 1.8 μM predicted for Fig. 4, Scheme 2B, using Eq. 12. The underlying reason that K_{App} is lower for Fig. 4, Scheme 2B, than Scheme 2A is that the reaction corresponding to the J_2 equilibrium constant provides additional relief of the 60% DTX substate (S_{DTX}) due to a significant level of DTX binding within the BPTI burst.

In summary, detailed analysis of single K_{Ca} channels shows that the ligand interaction between DTX-I and BPTI is not consistent with the pseudo one-site competition mechanism of Fig. 4, Scheme 2A. Most likely, additional state(s) of simultaneous binding of these two different Kunitz inhibitor molecules contribute to the observed behavior. At minimum, the results implicate the simultaneous binding of one DTX-I and one BPTI molecule on the tetrameric channel as represented in Fig. 4, Scheme 2B. It is also clear that there is a strongly antagonistic interaction between DTX-I and BPTI that lowers the affinity for binding of each ligand by a factor of ~11 in the doubly occupied state. This evidence for simultaneous but antagonistic ligand occupancy by BPTI and DTX-I provides an explanation for the mechanistic quandary posed at the beginning of the RESULTS; i.e., how can the interaction kinetics of BPTI with a nonpore site on a homotetrameric complex approximate one-site behavior. Despite this satisfying resolution, our experience with the practical limitations in collecting such data sets and the formidable kinetic complexities that would be faced in attempting to analyze the interaction of BPTI and DTX-I in greater detail dissuaded us from pursuing this system. Instead, we focused next on ligand interactions between DTX-I and a homologue of the *Shaker* ball peptide.

A Homologue of the Shaker Ball Peptide Exhibits Slow Blocking Activity Described by a One-Site Process

The evidence for simultaneous binding of BPTI and DTX-I presented above is compatible with the idea that the binding sites for these inhibitors are off-center from the pore, as it is difficult to envision that both of these large molecules with approximate dimensions of ~19 × 19 × 29 Å could simultaneously fit inside the central channel. As mentioned in the INTRODUCTION, previous work showed that internal Ba^{2+} readily blocks the BPTI-occupied channel, and internal TEA readily blocks the DTX-occupied channel (Lucchesi and Moczydlowski, 1991). The latter findings were actually the first indication that the binding sites for BPTI/DTX-I are not located within the pore. However, we wondered whether it might be possible to detect interactions between Kunitz inhibitors and pore blockers by using a larger blocking molecule. The *Shaker* ball peptide and its homologues are currently the largest molecules known to block K_V channels by binding within the pore. Fig. 5 A shows the sequence of the 20-residue NH_2 terminus of the *Shaker* K^+ channel of *Drosophila*

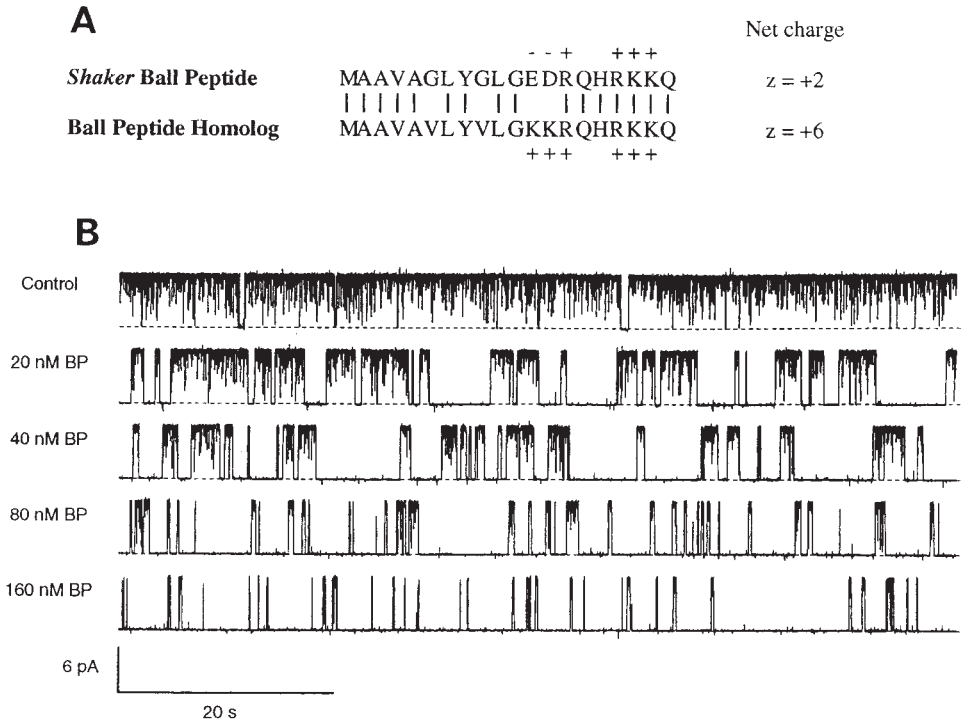

FIGURE 5. Titration of a single K_{Ca} channel with a homologue of *Shaker* ball peptide. (A) Primary sequences of the native *Shaker* ball peptide and a homologue (BP) also known as G6VG9VE12*K*D13K (Toro et al., 1994). (B) Representative current records from a K_{Ca} channel recorded under control conditions and after addition of 20, 40, 80, and 160 nM BP on the internal side. Voltage, +30 mV. The dashed line denotes zero current.

that mediates rapid inactivation by a ball-and-chain type of mechanism (Hoshi et al., 1990; Zagotta et al., 1990). Even though most maxi-K_{Ca} channels do not exhibit rapid inactivation and do not have a ball peptide sequence at the NH_2 terminus, the *Shaker* ball peptide is known to block maxi-K_{Ca} channels by a pore-occlusion mechanism (Foster et al., 1992; Toro et al., 1992). This finding has been explained by the idea that K_{Ca} channels possess a vestigial or surrogate receptor site for the ball peptide that confers sensitivity to block by such peptides. To investigate the relationship between the binding sites for Kunitz inhibitor proteins and the internal pore region, we studied the interaction between DTX-I and a ball peptide homologue.

The sequence of the particular ball peptide homologue that we chose for this study is shown in Fig. 5 A. The BP homologue has four amino acid substitutions of the native peptide, G6V, G9V, E12K, and D13K, that result in increased hydrophobicity and net positive charge ($z = +6$) compared with that of native BP ($z = +2$). This particular BP homologue was first described by Toro et al. (1994), who showed it has ~200-fold greater blocking affinity than the native *Shaker* ball peptide for a maxi-K_{Ca} channel from pig. Fig. 5 B shows the effect of titrating a single rat muscle K_{Ca} channel with BP homologue at +30 mV and 50 mM symmetrical KCl. The BP homologue induces the appearance of discrete blocking events of several seconds duration in the single channel record and the probability of this blocked state progressively increases with BP concentration over the range of 0–160 nM.

The kinetics of interaction of BP homologue with single K_{Ca} channels were analyzed by compiling dwell time histograms of blocked events and unblocked waiting times between adjacent blocked states. The probability histograms for these two types of events are well described by single-exponential functions. For example, Fig. 10 A shows a dwell time histogram of BP-blocked events plotted in the format of square root of events vs. log time. The binned dwell time data exhibits one predominant exponential component as shown by the superimposed fit. Fig. 6, A and B, plot mean lifetimes of the blocked state, τ_B, and the unblocked state, τ_U, as a function of the concentration of BP homologue. Fig. 6 A shows that τ_B is essentially independent of blocker concentration over the range of 10–160 nM peptide with a mean value of 1.71 ± 0.07 s (±SEM, $n = 6$). Fig. 6 B shows that τ_U is inversely related to the blocker concentration. The results of Figs. 6, A and B, are consistent with a simple reversible blocking reaction like that of Fig. 6, Scheme 3. Fig. 6, Scheme 3, demands the following relationships:

$$\tau_B = (b_{-1})^{-1} \quad (13)$$

$$\tau_U = (b_1[BP])^{-1} \quad (14)$$

$$P_U = \frac{B_1}{B_1 + [BP]}. \quad (15)$$

The mean lifetime of the BP-blocked events obtained from the data in Fig. 6 A yields a value of $b_{-1} = 0.585 \pm 0.025\ s^{-1}$ for the dissociation rate constant of BP accord-

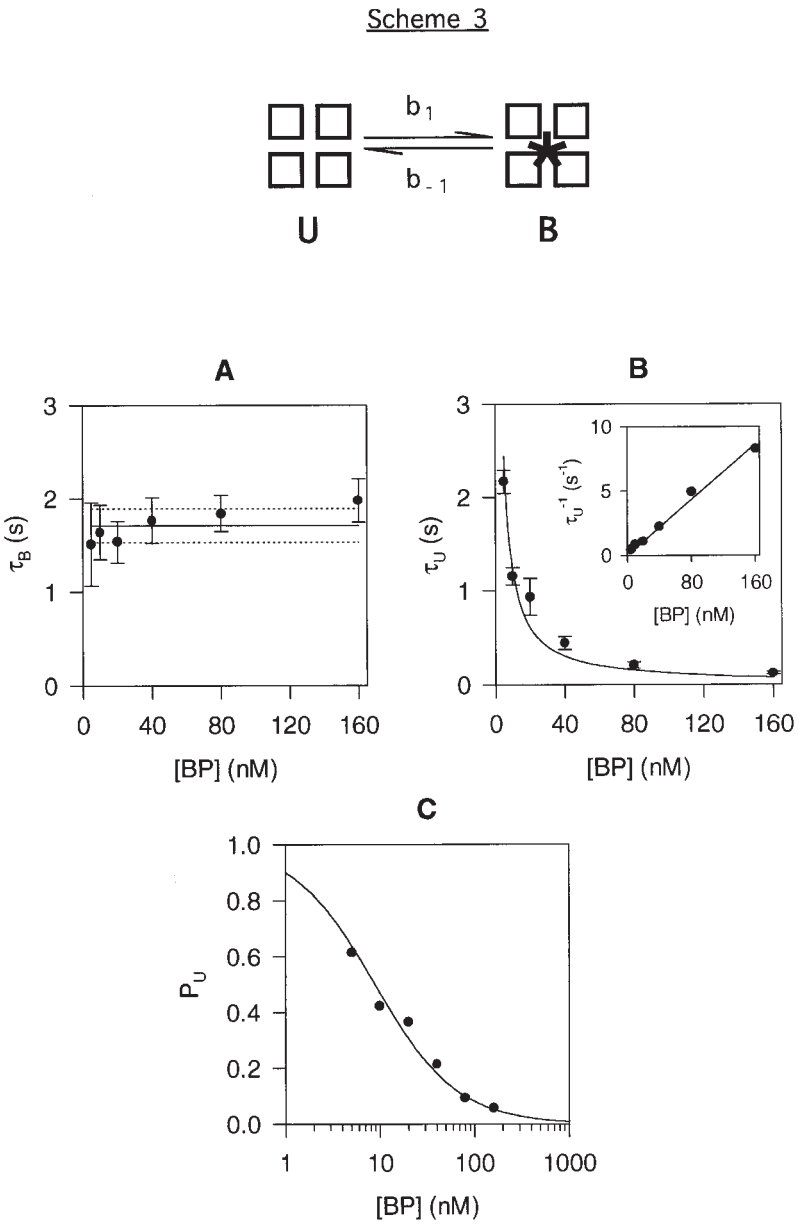

FIGURE 6. Analysis of BP blocking kinetics. Scheme 3 represents a binding reaction for the reversible association of BP with a single site in the K_{Ca} channel pore. □, unoccupied subunits; *, represents BP bound to the pore. The association rate constant of BP is b_1, and the dissociation rate constant is b_{-1}. U, the unoccupied state of the channel; B, the BP-blocked state. (A) Lifetime of the BP-blocked state as a function of [BP]. (B) Lifetime of dwell times between adjacent BP-blocked states as a function of [BP]. Data points and error bars in A and B are the mean ± SEM for three to seven single channels. The solid line and two dotted lines in A are the mean ± SD of the six data points used to measure b_{-1} from the lifetime τ_B of state B (Eq. 13). The solid line in B is a fit to Eq. 14 used to measure b_1 from the lifetime τ_U of state U. The inset shows the same data plotted as the reciprocal lifetime. (C) Time-averaged probability of a channel being in the unoccupied (BP-free) state as a function of BP. Each point was calculated from 4.5–6.5 h of data pooled from three to seven single channels. The solid line in C is a fit to Eq. 15 used to measure the equilibrium constant B_1 as described in the text.

ing to Eq. 13. The data of Fig. 6 B were fit to Eq. 14 to obtain a value of $b_1 = 8.17 \pm 0.73 \times 10^7\ s^{-1}M^{-1}$ for the bimolecular association rate constant of BP. The kinetic ratio of b_{-1}/b_1 gives a value of $B_1 = 7.16 \pm 0.71$ nM for the equilibrium dissociation constant of BP under these conditions. The assumption of a single class of binding sites for BP was also tested by plotting the time-averaged probability of the unblocked U state, P_U, vs. [BP] as shown in Fig. 6 C. A nonlinear fit of these data to Eq. 15 gives a value of $B_1 = 8.85 \pm 0.71$ nM, which closely agrees with the corresponding ratio of rate constants. Thus, the blocking behavior of the particular high-affinity BP homologue that we have studied is well described by a one-site blocking reaction. This blocking site is assumed to be located directly within the inner pore because the smaller pore-blocking molecule, TEA, inhibits ball peptide block of the maxi-K_{Ca} channel in a strictly competitive fashion (Toro et al., 1992). External K^+ has also been found to relieve the block by internal BP (Foster et al., 1992; Toro et al., 1992). We have also confirmed that internal TEA decreases the association rate of BP homologue in a competitive fashion under our conditions (data not shown). This characterization of a BP homologue as a pore blocker thus provides the groundwork for investigating ligand–ligand interactions between the Kunitz inhibitor site and the BP blocking site.

A Complex Pattern of Blocking Activity by Ball Peptide Homologue in the Presence of DTX-I Reflects Simultaneous Binding of Two Ligands

If the binding site for BP overlaps with that of DTX-I, then BP-blocking events should only interrupt dwell

time durations in the open state when the channel is unoccupied by DTX-I. Alternatively, if the binding site for BP is physically distinct from that of DTX-I, then BP-blocking events should also interrupt the long-lived DTX substate. The current records of Fig. 7 demonstrate that the latter alternative prevails. In this experiment, 460 nM DTX-I induced long-lived DTX-substate events that comprised ~97% of the time-averaged activity of a single K_{Ca} channel. Subsequent addition of 20 nM BP to the internal side resulted in a complex pattern of blocking activity consisting of four easily recognized types of discrete blocking events that can be defined on the basis of how they begin and end. Some of the discrete blocking events are flanked at both the entry and exit transitions by the DTX substate. This type of event would be expected to occur if BP binds to the DTX-occupied channel and dissociates again before DTX-I has a chance to dissociate. A second type of discrete blocking event is initiated from a DTX substate and is terminated by a transition to a fully open current level. This may correspond to an event in which BP first binds to a DTX-occupied channel, followed by electrically silent dissociation of DTX-I, and then by dissociation of BP. A third class of discrete blocking events are initiated from a fully open state and terminated by a transition to a DTX sublevel. This may correspond to a blocking event that starts with BP binding to an unoccupied channel, followed by the electrically silent binding of DTX-I to the fully blocked channel, and terminated by dissociation of BP from the DTX-occupied channel. The fourth type of blocking event begins and ends with the fully open state. This class of events would be expected to occur when BP binds and dissociates from the channel during periods when DTX is never bound. The latter events could also occur when BP binds to an unoccupied channel and DTX-I binds and then dissociates one or more times before BP finally dissociates. If the binding of another ligand to the BP-blocked state is presumed to be electrically silent, the various classes of blocked states described above could also reflect multiple numbers of silent DTX-I–binding events. This preliminary discussion of the single-channel behavior in the presence of DTX-I and BP points to a mechanism that involves simultaneous occupancy and unordered binding of these two ligands.

The Association Rate of Ball Peptide Homologue Is Slower when the Channel Is Occupied by DTX-I

To analyze this two-ligand system, we first measured the durations of the following two types of events: (a) unconditional BP-blocked events defined as any uninterrupted residence time in the fully blocked state, and (b) unconditional DTX-substate events defined as any uninterrupted residence time in the ~60% DTX-substate current level. Samples of these two types of events containing 50–350 dwell times were manually identified and pooled from five different single channel bilayers each at seven different concentrations of BP ranging from 5 to 320 nM. The simple arithmetical mean of these samples is plotted as a function of BP concentration in Fig. 8, A and B. Fig. 8 A shows that the mean unconditional dwell time of the BP-blocked state, τ_{BP}, is independent of [BP] and has a value of 4.62 ± 0.13 s (±SEM, $n = 7$) averaged over all BP concentrations. This result is inconsistent with one-site competition. Such a mechanism (Fig. 8, Scheme 4A) predicts that the lifetime of the BP-blocked state is equal to the reciprocal of the BP dissociation rate constant, $1/b_{-1}$, which was previously measured as 1.71 ± 0.07 s from the mean blocked time in the absence of DTX-I (Fig. 6 A). This comparison shows that average duration of the

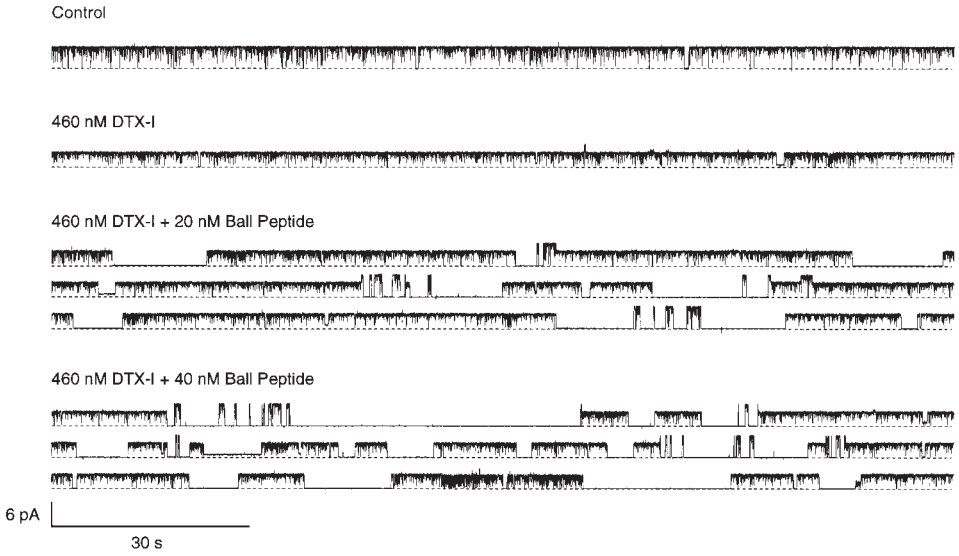

FIGURE 7. Representative records from a single K_{Ca} channel recorded in the presence of DTX-I alone and DTX-I plus two different concentrations of BP. The top trace was obtained under control conditions before addition of peptide and the second trace from the top was recorded after the addition of 460 nM DTX-I to the internal side of the bilayer. The next two groups of three traces are continuous segments of recordings taken after the addition of 20 and 40 nM internal BP, respectively, to the same channel. The dotted line marks the zero current level.

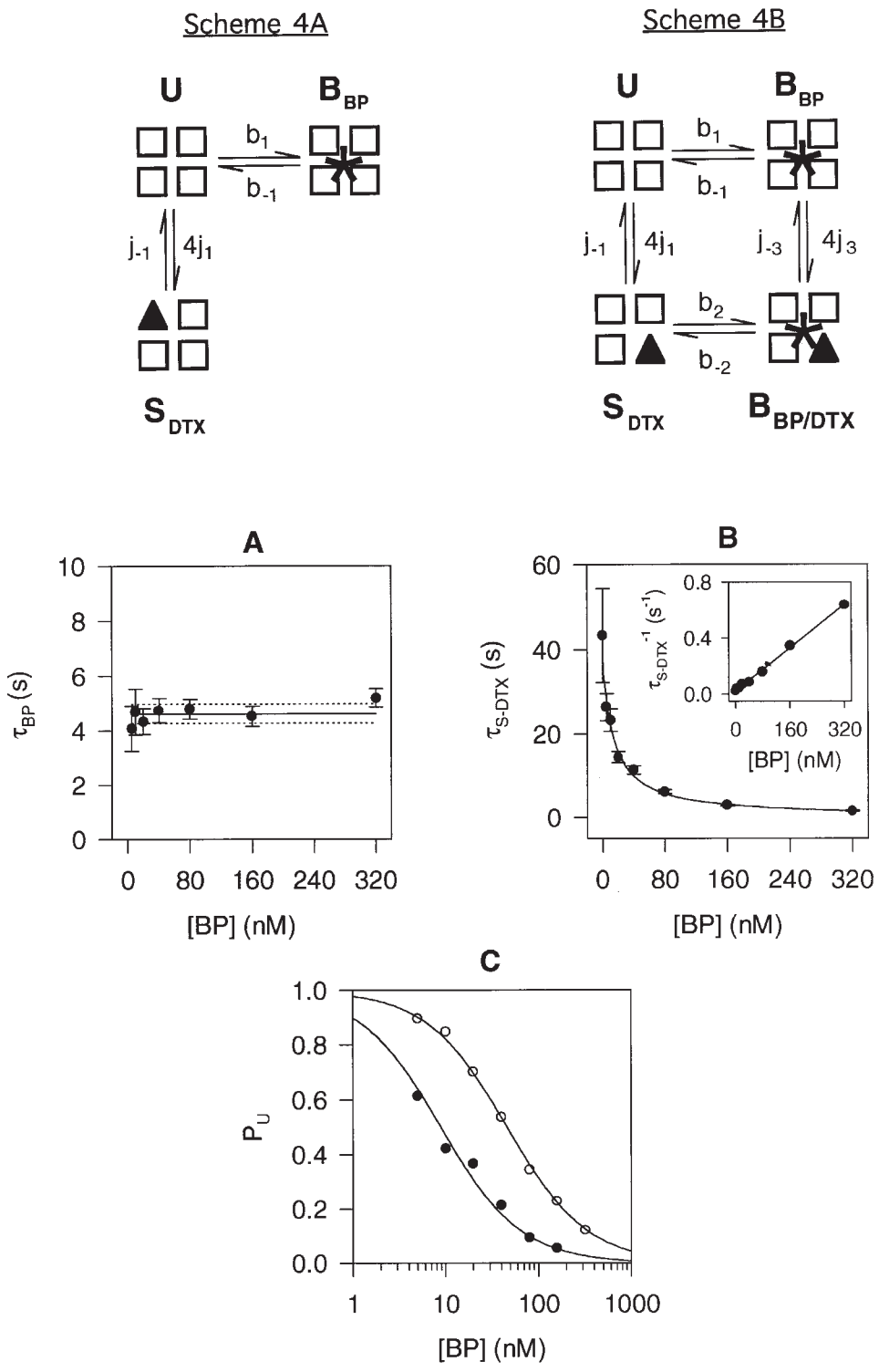

FIGURE 8. Kinetic analysis of ligand interactions between DTX-I and BP. Scheme 4A shows a hypothetical three-state model for simple binding competition between DTX-I and BP. This scheme would be expected to describe a situation where binding sites of two different ligands physically overlap. This model assumes that DTX-I can bind to only one of the four subunits at a time. □, unoccupied subunits; ▲, DTX-bound subunit; and *, BP bound to the pore. Scheme 4B shows a four-state model that describes binding of DTX-I to a nonpore site on any one subunit at a time and simultaneous binding of BP to a single site in the pore. U is the unoccupied state, S_{DTX} is the DTX-bound substate, B_{BP} is the BP-blocked state, and $B_{BP/DTX}$ is the doubly occupied blocked state. (A) Mean dwell time of the unconditional BP-blocked state as function of BP. Events identified as fully blocked states were pooled from five different single K_{Ca} channels at each concentration of BP. The pooled samples contained from 67 to 899 events. The data points and error bars correspond to the arithmetic mean ± SEM. The solid line and two dotted lines correspond to the mean ± SEM of the seven data points used to calculate the J_3 equilibrium constant from Eq. 19. (B) Measured lifetime of the DTX substate as a function of BP concentration. Events identified as uninterrupted dwell times in the DTX substate were pooled from five different K_{Ca} channels at each concentration of BP. These samples containing 50–328 events were well-described by simple exponential distributions. Data points represent the arithmetic mean ± SEM of these samples. The solid line is a fit to Eq. 16 that was used to measure the rate constant, b_2. (Inset) The same data plotted as the reciprocal of the mean dwell time. (C) Measured probability that the channel is not occupied by BP as a function of [BP]. ●, data in the absence of DTX-I, also shown in Fig. 6 C; ○, data in the presence of 460 nM DTX-I. Each point was calculated from 0.7–1.5 h of data pooled from five K_{Ca} channels. The solid line drawn through these points is a fit to Eq. 17, using K_{App} = 45.9 nM, which was used to calculate B_2 according to Eq. 18.

BP-blocked state is increased by a factor of 4.62/1.71 s = 2.7 in the presence of 460 nM DTX-I vs. the absence of DTX-I. Fig. 8, Scheme 4A, also predicts that the unconditional lifetime of the DTX substate is equal to the reciprocal of the DTX-I dissociation rate constant, $1/j_{-1}$, and is independent of [BP]. This is inconsistent with the results of Fig. 8 B, which show that the mean unconditional dwell time of the DTX substate varies in-

versely with [BP]. Thus, two major predictions of Fig. 8, Scheme 4A, are clearly violated, ruling out an overlapping binding site for BP and DTX-I.

Fig. 8, Scheme 4B, is a cyclic four-state model that allows for the unordered and simultaneous binding of BP and DTX-I to distinct sites. Since there is only one state with a current level at the DTX-substate, S_{DTX}, this model predicts that the unconditional mean dwell time of the DTX substate is equal to the reciprocal of the sum of the rates for leaving this state:

$$\tau_{S-DTX} = (j_{-1} + b_2[BP])^{-1}. \quad (16)$$

Eq. 16 describes the observed shortening of the mean duration of the DTX substate with increasing [BP]. A nonlinear fit of the data in Fig. 8 B to Eq. 16 using the previously established value of $j_{-1} = 0.0266\ s^{-1}$, yields $1.85 \pm 0.30 \times 10^6\ s^{-1}M^{-1}$ for the parameter, b_2, which is the bimolecular association rate constant for binding of BP to the DTX-occupied substate. Comparison of b_2 with b_1 measured above (see Table I) shows that the association rate constant for binding of BP to the DTX-occupied channel is 44-fold slower than that for binding of BP to the unoccupied channel.

The Rate of BP Dissociation Is also Slower when the Channel Is Occupied by DTX-I

Additional information on the interaction of BP and DTX-I can be obtained from measurements of the time-averaged probability of the BP-blocked state. As described above for experiments in the absence of DTX-I, the probability that the channel is not blocked by BP follows a titration curve with an apparent dissociation constant of 8.85 ± 0.71 nM, which is an estimate of the equilibrium dissociation constant, B_1. This data and fit is reproduced (Fig. 8 C, ●). We similarly computed the probability that the channel is not blocked by BP for single channel records in the presence of 460 nM DTX and is plotted (Fig. 8 C, ○). The rightward shift of this data to higher BP concentrations provides another quantitative measurement of the interaction between BP and DTX-I. The following equations derived from Fig. 8, Scheme 4B, give the form of theoretical dependence of the probability, $P_{not\ BP}$, that the channel is not in either of the two BP-blocked states, B_{BP} and $B_{BP/DTX}$, as a function of BP concentration:

$$P_{notBP} = \frac{K_{App}}{K_{App} + [BP]} \quad (17)$$

$$K_{App} = \frac{\left(1 + \frac{[DTX]}{J_1}\right)}{\left(\frac{1}{B_1} + \frac{[DTX]}{J_1 B_2}\right)}. \quad (18)$$

The data of Fig. 8 C corresponding to BP titrations in the presence of 460 nM DTX-I (○) were fit to Eq. 17 to obtain a value of $K_{App} = 45.9 \pm 1.5$ nM. Since J_1, B_1, and [DTX] are already known from calculations presented above, Eq. 18 can be solved to obtain an estimate for the equilibrium constant, B_2. This calculation yields $B_2 = 57.0 \pm 8.6$ nM, which indicates that BP binds to the DTX substate with 8.0 ± 1.6-fold lower affinity than to the unoccupied channel (see Table I).

Since the values of the bimolecular rate constant b_2 and the equilibrium constant B_2 have now been obtained, the dissociation rate constant b_{-2} can be estimated from the relation, $b_{-2} = b_2 B_2$. This calculation yields a value of $b_{-2} = 0.105 \pm 0.023\ s^{-1}$ and reveals the surprising result that BP dissociates 5.6 ± 1.2-fold more slowly from the DTX-bound channel than from the unoccupied channel (see Table I). In other words, our analysis shows that, although DTX-I lowers the affinity of BP by a factor of ~8 at equilibrium, it actually stabilizes the BP-bound state of the channel by slowing the rate of BP dissociation. The inhibition of BP binding by DTX-I at equilibrium is solely due to the 44-fold inhibitory effect of DTX-I on the association rate of BP.

If the rate of dissociation of BP from the DTX-occupied channel is calculated to be 5.6-fold slower than that in the absence of DTX-I, why is the average dwell time of the BP-blocked state only increased by 2.7-fold over that in the absence of DTX-I (i.e., Fig. 8 A)? Fig. 8, Scheme 4B, actually has two BP-blocked states, B_{BP} and $B_{BP/DTX}$, that are functionally indistinguishable by unitary current. According to principles of Markov processes, the reciprocal mean dwell time of the group of these two indistinguishable states, τ_{BP}, is given by the sum of the two rate constants, b_{-1} and b_{-2}, for leaving this group, with each of these rate constants weighted by the fraction of the group in the respective exit state, B_{BP} or $B_{BP/DTX}$, at equilibrium. This relationship leads to the following formula for τ_{BP}:

$$\tau_{BP} = \frac{\left(1 + \frac{[DTX]}{J_3}\right)}{\left(b_{-1} + \frac{b_{-2}[DTX]}{J_3}\right)}. \quad (19)$$

Eq. 19 predicts the experimental result that the mean dwell time of the grouped BP-blocked state is independent of BP concentration. Since numerical estimates of the rate constants, b_{-1} and b_{-2}, are available from calculations already described above, the value of $\tau_{BP} = 4.63 \pm 0.35$ s (Fig. 8 A) may be used to compute J_3, the equilibrium dissociation constant for binding of DTX-I to the BP-blocked state, directly from Eq. 19. This calculation yields $J_3 = 139 \pm 34$ nM. Since the equilibrium dissociation constants B_1, B_2, J_1, and J_3 have now all been independently obtained from various single-channel measurements on the system, the microscopic reversibility of Fig. 8, Scheme 4B, can be checked from the following relationship:

$$\frac{J_3}{J_1} = \frac{B_2}{B_1}. \quad (20)$$

Using the values for J_1, J_3, B_1, and B_2 listed in Table I, the left hand side of Eq. 20, J_3/J_1, is equal to 8.4 ± 2.2, and the right hand side of Eq. 20, B_2/B_1, is equal to 8.0 ± 1.4. These ratios are equivalent within the propagated error of the measurements. This further supports the use of Fig. 8, Scheme 4B, as an appropriate model for this ligand–ligand interaction. According to this model, the 2.7-fold increase in the average lifetime of the apparent BP-blocked state (Fig. 8 A) originates from the slower rate of BP dissociation from the DTX-bound state (b_{-2}) compared with the unoccupied channel (b_{-1}), and the DTX-binding equilibrium constant, J_3, which determines the fraction of the grouped BP-blocked state that exists as B_{BP} or $B_{BP/DTX}$.

Transition Probabilities for the BP-blocked State in the Presence of DTX-I Show that the Ligand Interaction Is in Thermodynamic Equilibrium

The single-channel records of Fig. 7 indicate that the BP-blocked state can either be entered from the unoccupied state of the channel or directly from the DTX substate. Fig. 8, Scheme 4B, can be used to calculate the predicted time-averaged probability of these two types of events. $P_{entry,U}$ may be defined as the probability that the grouped BP-blocked state is entered directly from the unoccupied U state versus the S_{DTX} substate. This probability is computed as a ratio of the rate that a channel will transit from the U state to the B_{BP} state over the sum of the rates for transiting from state U to B_{BP} and from state S_{DTX} to $B_{BP/DTX}$. Following from Fig. 8, Scheme 4B, the numerator of this ratio is equal to the product of the association rate constant (b_1), the concentration of BP ([BP]), and the equilibrium fraction f_U of states U and S_{DTX} that is in the U state, where $f_U = J_1/(J_1 + [DTX])$. Similarly, the denominator of this ratio is equal to $b_1[BP]f_U + b_2[BP]f_{S\text{-}DTX}$, where $f_{S\text{-}DTX}$ is equal to $[DTX]/(J_1 + [DTX])$. Algebraic simplification of the expression for this ratio leads to the following formula for $P_{entry,U}$:

$$P_{entry,\,U} = \frac{b_1 J_1}{b_1 J_1 + b_2[DTX]}. \quad (21)$$

Using the estimated values of b_1, b_2, and J_1 listed in Table I and [DTX] = 460 nM, $P_{entry,\,U}$ as calculated from Eq. 21 is equal to 0.61 ± 0.13. Fig. 9 A plots experimentally determined values of $P_{entry,\,U}$ measured from single channel records in the presence of 460 nM DTX at different BP concentrations in the range of 10–320 nM. The figure shows that the measured probability of entering the BP-blocked state from the unoccupied U state is independent of BP concentration, as expected from Eq. 21. The average measured value of $P_{entry,\,U}$ = 0.58 ± 0.06 is not significantly different from the value of 0.61 ± 0.13 predicted from the relationship of Eq. 21.

The single-channel records of Fig. 7 also show that the channel can exit from the BP-blocked state either directly to the fully open state or to the DTX substate. Using similar reasoning as that described for the conditional probability of entering the BP-blocked state, Fig. 8, Scheme 4B, can be used to derive the following theoretical formula for $P_{exit,\,U}$, which is defined as the time-averaged probability for exiting the grouped BP-blocked state directly to the unoccupied U state vs. the S_{DTX} substate:

$$P_{exit,\,U} = \frac{b_{-1} J_3}{b_{-1} J_3 + b_{-2}[DTX]}. \quad (22)$$

TABLE I

Summary of Kinetic Parameters for the Ligand Interaction between DTX-I and BP as Defined by Fig. 8, Scheme 4B

Ligand	Dissociation rate constant	Association rate constant	Equilibrium dissociation constant
	s^{-1}	$s^{-1}M^{-1}$	nM
DTX-I	from S_{DTX}	to U	from S_{DTX}
	$j_{-1} = 0.0266 \pm 0.0015$*	$4j_1 = 1.61 \pm 0.11 \times 10^6$‡	$J_1 = 16.5 \pm 1.4$§
DTX-I	from $B_{BP/DTX}$	to B_{BP}	from $B_{BP/DTX}$
	$j_{-3} = 0.11 \pm 0.22$‖	$4j_3 = 1.20 \pm 0.38 \times 10^6$‖	$J_3 = 139 \pm 34$¶
	$j_{-3} = 0.17 \pm 0.07$**		
BP	from B_{BP}	to U	from B_{BP}
	$b_{-1} = 0.585 \pm 0.025$‡‡	$b_1 = 81.7 \pm 7.3 \times 10^6$§§	$B_1 = 7.16 \pm 0.71$‖‖
			$B_1 = 8.85 \pm 0.71$¶¶
BP	from $B_{BP/DTX}$	to S_{DTX}	from $B_{BP/DTX}$
	$b_{-2} = 0.105 \pm 0.023$***	$b_2 = 1.85 \pm 0.30 \times 10^6$‡‡‡	$B_2 = 57.0 \pm 8.6$§§§

*Measured from $\tau_{S\text{-}DTX}$, Eq. 3; ‡measured from τ_U, Eq. 4; §calculated from $J_1 = j_{-1}/4j_1$; ‖measured from τ_1 and τ_2, Eqs. 23 and 24; ¶measured from τ_{BP}, Eq. 19; **calculated from $j_{-3} = (J_3)(4j_3)$; ‡‡measured from τ_B, Eq.13; §§measured from τ_U, Eq. 14; ‖‖calculated from $B_1 = b_{-1}/b_1$; ¶¶measured from P_U vs. [BP], Eq. 15; ***calculated from $b_{-2} = (B_2)(b_2)$; ‡‡‡measured from $\tau_{S\text{-}DTX}$, Eq. 16; §§§measured from $P_{not\ BP}$ vs. [BP], Eqs. 17 and 18.

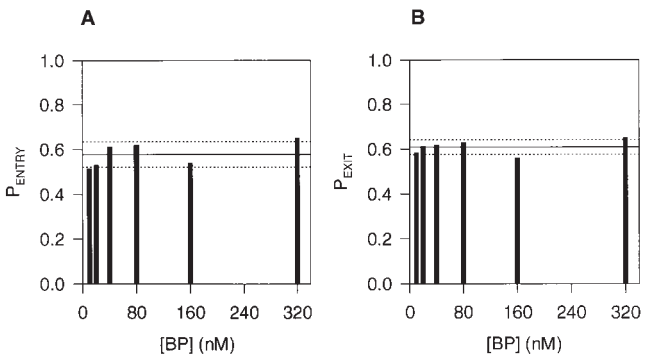

FIGURE 9. Transition probabilities for entry to or exit from the BP-blocked state. (A) Entry probability that the BP-blocked state is entered from the fully open or unoccupied state of the channel vs. the DTX substate. Transitions from the unoccupied U state to the BP-blocked state (B_{BP}) and from the DTX substate (S_{DTX}) to the BP-blocked state ($B_{BP/DTX}$) were counted for five single K_{Ca} channels at six concentrations of BP. The pooled data consisted of samples of 72–583 events at each BP concentration. The heights of the solid bars represent the fraction of total transitions that began from the unoccupied state. (B) Exit probability that the BP-blocked state (B_{BP} and $B_{BP/DTX}$) exits to the fully open state vs. the DTX substate. Similar to A, the heights of the solid bars represent the fraction of total transitions that exit to the unoccupied state. In A and B, the horizontal solid and dotted lines correspond to the mean ± SD of six different measurements. The computed means were used to check the predictions of Scheme 4B according to Eqs. 21 and 22, for A and B, respectively.

Substitution of the values of b_{-1}, b_{-2}, and J_3 from Table I, and using [DTX] = 460 nM, we find that $P_{exit,\,U} = 0.63 \pm 0.24$ as calculated from Eq. 22. In Fig. 9 B, we have plotted experimental values of $P_{exit,\,U}$ measured at various concentrations of BP ranging from 10 to 320 nM. Again, we see that this probability is independent of BP concentration, as expected from Eq. 22. We also find that the mean experimental value of $P_{exit,\,U} = 0.61 \pm 0.03$ is indistinguishable from the predicted value of 0.63 ± 0.24.

In analyzing the preceding time-averaged transition probabilities, we have purposely measured probabilities for two types of transitions that involve the same step ($U \leftrightarrow B_{BP}$) in Fig. 8, Scheme 4B, but in opposite directions, namely the entry probability ($P_{entry,\,U}$) for moving from state U to state B_{BP} and the exit probability ($P_{exit,\,U}$) for moving from state B_{BP} to state U. If the system is in thermodynamic equilibrium, then for any step in the cycle, the probability for moving in the forward direction must be equal the probability for moving in the reverse direction (Colquhoun and Hawkes, 1995). This is a hallmark feature of purely reversible Markov processes. The theoretical expressions of Eqs. 21 and 22 can be readily demonstrated to be mathematically equivalent by algebraic manipulation and use of the microscopic reversibility relationship of Eq. 20. The actual data presented in Fig. 9, A and B, show that $P_{entry,\,U}$ equals $P_{exit,\,U}$ within statistical limits of uncertainty. Thus, our analysis of BP transition probabilities is fully consistent with the expectations of Fig. 8, Scheme 4B.

Rate Constants for DTX-I Binding to the BP-blocked State Can Be Derived from Time Constants of the Double-Exponential Dwell Time Distribution of all BP-blocked Events

Thus far, our analysis has provided estimates for all of the individual rate constants of Fig. 8, Scheme 4B, except $4j_3$ and j_{-3}, which are the respective association and dissociation rate constants of DTX-I binding to the BP-blocked state. These parameters can be determined from the complex dwell time distribution of all BP-blocked events. Since the BP-blocked state (B_{BP}) is indistinguishable from the BP-blocked state occupied by DTX-I ($B_{BP/DTX}$) on the basis of unitary current, the distribution of all blocked events represents sojourns in both of these states and the probability distribution of all BP-blocked states for Fig. 8, Scheme 4B, is predicted to be a sum of two exponentials. Since these two blocked states are in direct communication and can undergo interconversion, the observed lifetimes of the two exponentials will be complex functions of j_{-3}, $4j_3$, and [DTX], parameters that govern the interconversion of B_{BP} and $B_{BP/DTX}$, plus the two rate constants for leaving the grouped block state, b_{-1} and b_{-2}. Theoretical expressions for the blocked state probability distribution of Fig. 8, Scheme 4B, can be derived by mathematical methods previously described in the channel literature (Pietrobon et al., 1989). The resulting sum-of-two-exponentials function is characterized by two time constants, τ_1 and τ_2, that must satisfy the following two equations:

$$\tau_1^{-1} + \tau_2^{-1} = 4j_3[\mathrm{DTX}] + j_{-3} + b_{-1} + b_{-2} \qquad (23)$$

$$(\tau_1\tau_2)^{-1} = j_{-3}b_{-1} + b_{-1}b_{-2} + 4j_3[\mathrm{DTX}]b_{-2}. \qquad (24)$$

Fig. 10 shows dwell time histograms of BP-blocked events compiled from single maxi-K_{Ca} channels in the absence (A) and presence (B) of 460 nM DTX-I. As discussed earlier, the histogram of BP-blocked events in the absence of DTX-I is well described by a single exponential component with a time constant of 1.73 s, which is equal to the mean dwell time of BP-blocked events measured over a wide range of BP concentration (Fig. 6 A). In contrast, the histogram compiled in the presence of DTX-I is described by a sum-of-two-exponentials with a short time constant of 0.90 s and a long time constant of 6.22 s. If average determinations of these latter two values are substituted for τ_1 and τ_2 in Eqs. 23 and 24, and other measurements (Table I) are substituted for b_{-1} and b_{-2}, this leaves us with two equations in two unknowns that may be solved simultaneously for $4j_3$ and j_{-3}. The results of this calculation

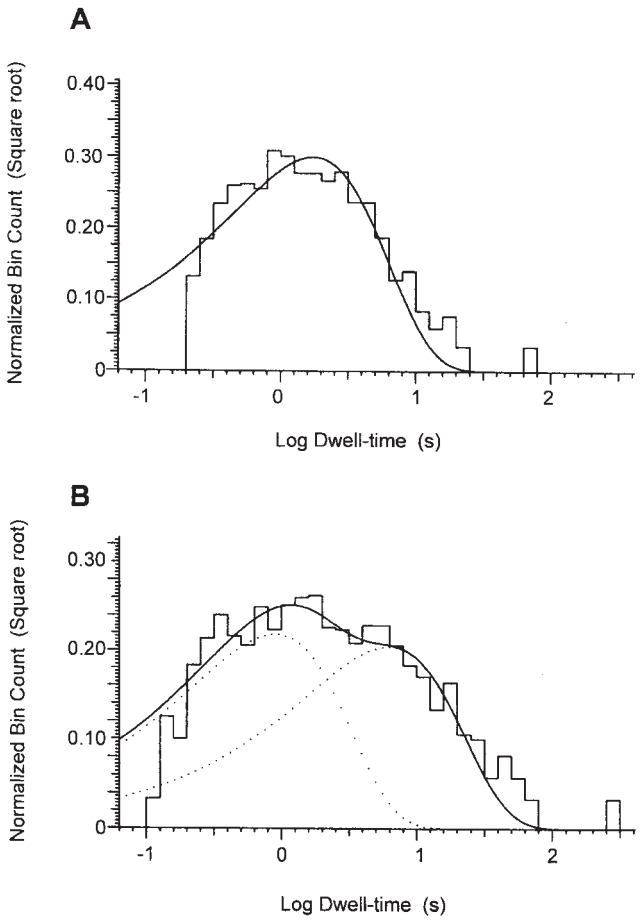

FIGURE 10. Probability density histograms of BP-blocked events recorded in the absence and presence of DTX-I. (A) Dwell time histogram of blocked events recorded from single K_{Ca} channels in the presence of 160 nM BP. Blocked events from seven different single K_{Ca} channels were pooled to obtain a sample of 857 events. The sample of events was binned and plotted according to the method of Sigworth and Sine (1987) using the square root versus log time format. The solid line is a fit of the data to a single exponential with a time constant of 1.73 s. (B) Dwell-time histogram of blocked events recorded in the presence of 460 nM DTX-I plus 160 nM BP. The sample contains 899 events pooled from five single K_{Ca} channels. The solid line is a fit to a sum-of-two-exponentials function with a short time constant of 0.90 s (amplitude, 0.53) and a long time constant of 6.22 s (amplitude, 0.47).

are: $4j_3 = 1.2 \pm 0.38 \times 10^6\ s^{-1}M^{-1}$ and $j_{-3} = 0.11 \pm 0.22\ s^{-1}$. Comparison of these latter values with $4j_1$ and j_{-1} (Table I), respectively, reveals that occupation of the channel by the ball peptide homologue only slows the apparent association rate of DTX-I by a factor of ~1.3-fold and increases the dissociation rate of DTX-I by a factor of ~4.1-fold.

Unfortunately, the use of Eqs. 23 and 24 to compute j_{-3} gives rise to a rather large propagated error on the value of this parameter, because it is calculated as the difference of two larger numbers, each with a substantial error. Thus, j_{-3} is the least certain parameter of the various rate constants determined for Fig. 8, Scheme 4B. Since the values of J_3 and $4j_3$ are known with greater precision, we have also calculated j_{-3} from the relationship, $j_{-3} = (J_3)(4j_3)$. This calculation gives $j_{-3} = 0.17 \pm 0.07\ s^{-1}$ and leads to the revised statement that BP increases the dissociation rate of DTX-I by ~6.3-fold (rather than ~4.1-fold).

Lack of Binding Interactions between the Internal Site(s) for DTX-I and the External Sites for TEA and Charybdotoxin

The results presented thus far reveal significant negatively coupled interactions between BPTI, DTX-I, and a ball peptide homologue that all bind at the intracellular face of maxi-K_{Ca} channels. To examine whether such interactions also occur between a peptide ligand on the intracellular side of the K_{Ca} channel and another ligand on the extracellular side, we measured block by external TEA or external ChTX in the absence and presence of internal DTX-I. Fig. 11 A shows the effect of increasing the concentration of TEA on the external side of a single K_{Ca} channel from 0 to 800 μM. The progressive decrease in amplitude of the unitary current observed as a function of TEA is consistent with previous studies that have described the fast blocking effect of this cation. At the single-channel level, "fast block" is observed whenever the dissociation rate of a blocking molecule is too brief to be resolved by the recording system (e.g., Moczydlowski, 1992). If the apparent single-channel current is normalized to the unblocked current and plotted as a function of external TEA concentration, the results are well described by a single-site titration curve with a K_d of 190 ± 37 μM (Fig. 11 C). Fig. 11 B shows records of a similar experiment on a different maxi-K_{Ca} channel in the presence of 460 nM DTX-I. If TEA binds with lower affinity to the DTX-occupied channel, then one would have expected the DTX substate to be less sensitive to the fast blocking effect of external TEA. The normalized apparent unitary current of the DTX substate is also plotted in Fig. 11 C as a function of external [TEA]. The data is well described by a single-site titration curve with a K_d of 257 ± 10 μM. Although there is a small increase in the K_d for TEA for the DTX substate vs. the unmodified channel, the difference is not statistically significant ($P = 0.1$). Thus, there is no detectable binding interaction between internal DTX-I and external TEA.

A similar experiment was performed with internal DTX-I and external ChTX. ChTX is a slow-blocking K^+ channel toxin with a binding site localized to the outer vestibule and pore entrance (MacKinnon et al., 1998). Fig. 12 (top three traces) shows current records of a single K_{Ca} channel in the presence of 10 nM ChTX. Previous studies have shown that the long-lived blocking events correspond to individual dwell times of ChTX on the channel and the unblocked events corre-

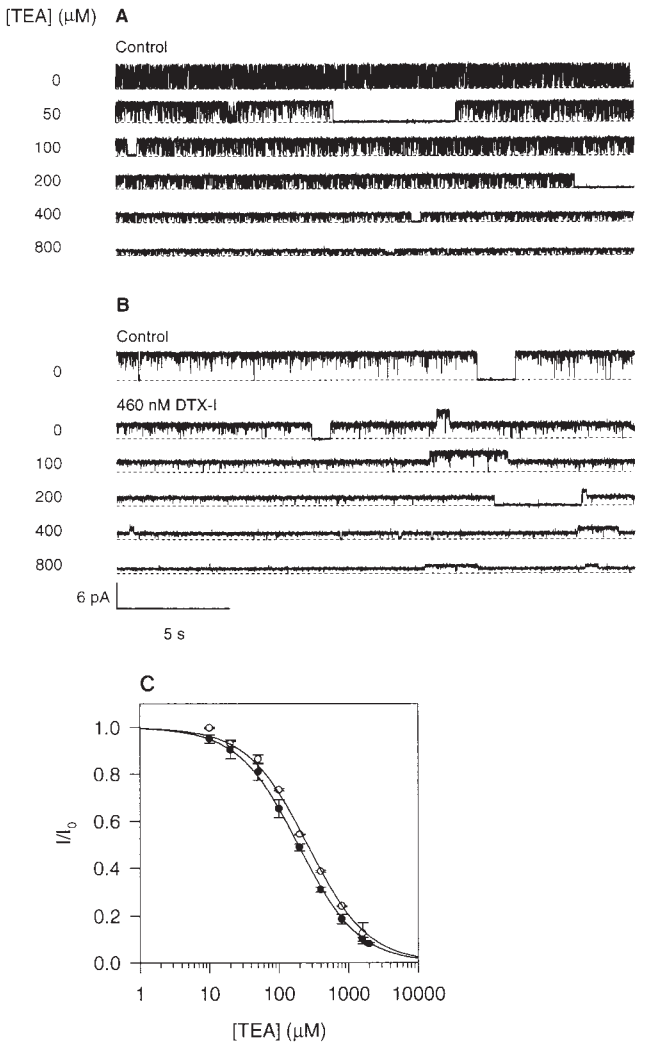

FIGURE 11. Titration of a single K_{Ca} channel with external TEA in the absence and presence of DTX-I. (A) Representative records from an experiment where a single K_{Ca} channel was exposed to a series of increasing TEA concentrations from 50 to 800 μM on the external side. Dotted lines mark the zero current level. (B) Representative records from an experiment where a single K_{Ca} channel was exposed to a series of increasing external TEA concentrations in the presence of 460 nM internal DTX-I. (C) Ratio of the unitary current of the open state (●) and the DTX-substate (○) as a function of external [TEA]. Data points are the mean ± SEM of three channels for the open state and two for the DTX substate. Solid lines are fits to a one-site binding isotherm as described in the text.

spond to waiting times between blocking events (Miller et al., 1985; Anderson et al., 1988). Such data can be analyzed in the manner described above for BP to obtain dissociation (k_{off}) and association (k_{on}) rate constants for ChTX. The results of this analysis are: k_{off} = 0.0369 ± 0.0004 s^{-1} and k_{on} = 2.77 ± 0.42 × 10^7 $s^{-1}M^{-1}$. The ratio of k_{off}/k_{on} gives a calculated K_d of 1.33 ± 0.20 nM for ChTX in the absence of DTX-I. Typical current records from the same K_{Ca} channel in the presence of 460 nM internal DTX are also presented in Fig. 12 (bottom three traces). Although the unblocked periods between ChTX blocking events have a lower unitary amplitude due to the DTX substate, the mean durations of the blocked and unblocked dwell times are very similar to those recorded in the absence of DTX-I. Quantitative analysis of the ChTX-blocked and unblocked dwell times gives the following rate constants for ChTX in the presence of DTX-I: k_{off} = 0.0350 ± 0.0003 s^{-1} and k_{on} = 2.89 ± 0.51 × 10^7 $s^{-1}M^{-1}$. The corresponding ratio of k_{off}/k_{on} gives a value of 1.21 ± 0.21 nM for the K_d of ChTX binding to the DTX-occupied channel. Comparison of these data with those cited above for ChTX alone shows that there is no significant difference between the rate constants for ChTX binding in the absence and presence of DTX-I. Thus, there is no detectable binding interaction between internal DTX-I and external ChTX.

DISCUSSION

In this study, we used planar bilayer recording and single-channel analysis to investigate the physical relationship of binding sites for two Kunitz inhibitor proteins (BPTI and DTX-I) and a homologue of the *Shaker* ball peptide on the intracellular side of a maxi-K_{Ca} channel. At the membrane voltage (+30 mV) and intracellular Ca^{2+} concentration (200 μM) used for these experiments, the K_{Ca} channel gating equilibrium is poised strongly toward the open state. Under these conditions, practically all of the channel closures due to normal gating are briefer than ~100 ms. The much slower association and dissociation kinetics of three different peptide ligands can be readily monitored by discrete changes in the unitary current record. Binding of BPTI and DTX-I produce distinct types of "substate" events and binding of BP produces discrete blocked states. The fact that each of these three ligands produces a different type of current signal upon binding to the channel allows us to identify events that are likely to arise from the simultaneous binding of two different ligands. Thus, the microscopic kinetics of complex ligand–ligand interactions are directly accessible in a single experiment. Analysis of such data allows us to discriminate a simple competitive interaction based on binding to physically overlapping sites from more complex types of interactions that involve simultaneous binding.

The Binding Site for Kunitz Inhibitor Proteins Is Located Outside of the Pore

In this work, we presented two new lines of evidence that BPTI and DTX-I do not bind within the internal ion conduction pathway or directly occlude the pore: (a) simultaneous binding of two Kunitz inhibitors, and (b) block of the DTX-occupied channel by a ball peptide homologue.

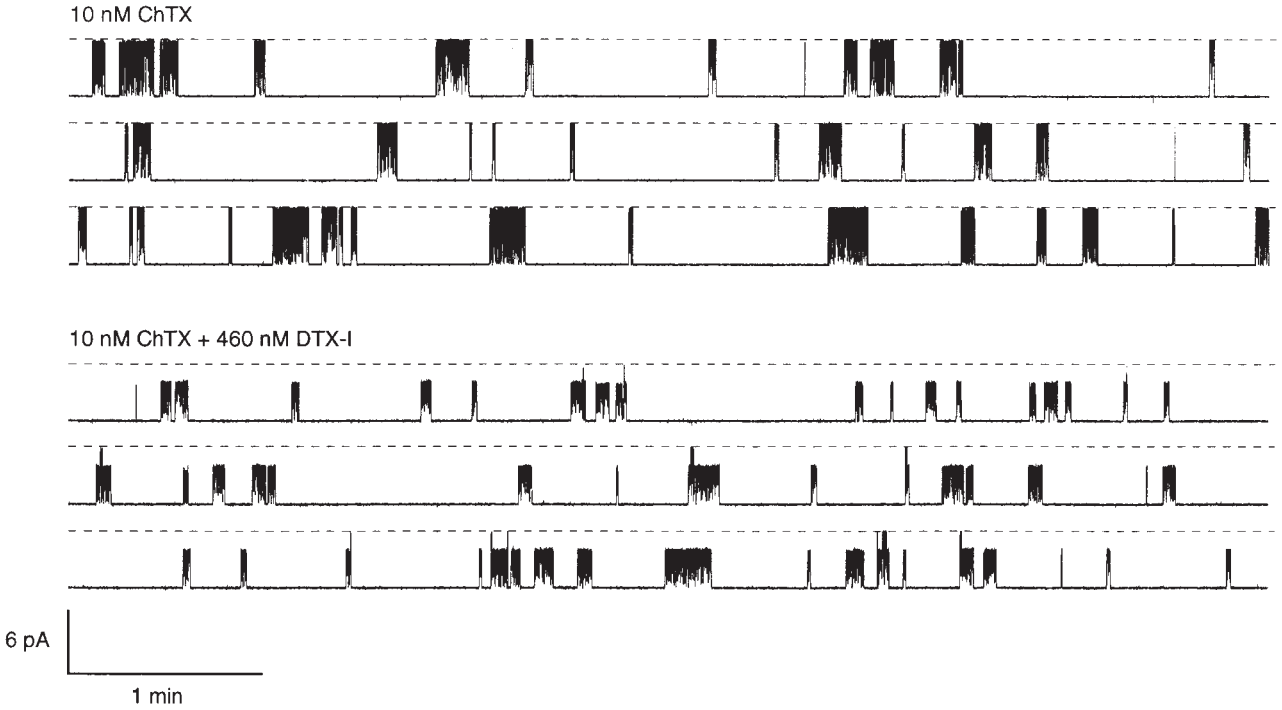

FIGURE 12. Effect of internal DTX-I on the blocking kinetics of external ChTX. Each group of three traces is a continuous segment of a recording from the same single K_{Ca} channel. The top records were recorded in the presence of 10 nM external ChTX and the bottom records were recorded after addition of 460 nM DTX-I to the internal side. Blocked and unblocked dwell-time events were measured and analyzed to determine the association and dissociation rate constants of ChTX as described in the text.

The evidence for simultaneous binding of BPTI and DTX-I is discussed below in more detail. Because BPTI and DTX-I have approximate dimensions of 19 × 19 × 29 Å, it is a priori unlikely that two of these molecules could simultaneously occupy distinct sites within the pore. Based on current knowledge of K^+ channel pore structure and tetrameric design (Doyle et al., 1998), our finding of a negatively coupled ligand–ligand interaction between BPTI and DTX-I is best explained by a model that involves one potentially available binding site for Kunitz inhibitors located on each of the four monomers of the K_{Ca} channel tetramer.

The first 20 NH_2-terminal residues of the *Shaker* B K^+ channel are directly involved in an N-type inactivation process that is referred to as a "ball and chain" mechanism. Much evidence supports the hypothesis that the tethered amino terminus or "ball domain" binds to the internal pore of the open *Shaker* channel and directly blocks K^+ current resulting in inactivation (Hoshi et al., 1990; Zagotta et al., 1990). Synthetic peptides corresponding to such ball domains of various voltage-gated K^+ channels and β subunits of K^+ channels have been found to mimic this inactivation process when added to channels that have been rendered defective in normal N-type inactivation (Demo and Yellen, 1991; Ruppersberg et al., 1991; Murrell-Lagnado and Aldrich, 1993b; Rettig et al., 1994). The primary evidence that such peptides directly block the *Shaker* pore is that ball peptide block is competitive with internal TEA and that external K^+ antagonizes binding of internal ball peptide (Murrell-Lagnado and Aldrich, 1993a,b).

Shaker ball peptide also blocks other types of ion channels that are more distantly related to voltage-gated K^+ channels, such as maxi-K_{Ca} and cyclic nucleotide–gated channels (Foster et al., 1992; Toro et al., 1992; Kramer et al., 1994). Although maxi-K_{Ca} channels do not exhibit N-type inactivation, block of these latter channels by ball peptide is functionally analogous to block of voltage-gated K^+ channels with respect to competition by internal TEA and antagonism by external K^+. This observation has been used to argue that maxi-K_{Ca} channels possess a similar kind of receptor site for BP as that of the *Shaker* K^+ channel. The particular BP homologue used in this study was chosen for its high affinity conferred by replacement of two acidic residues (Glu12 and Asp13) with Lys and replacement of two Gly residues (Gly6 and Gly9) with Val (Fig. 5 A). Although the native *Shaker* BP does not have a well-defined conformation in solution, there is evidence that residues 3–15 tend to adopt an α-helical structure that is further stabilized by replacement of Gly residues with Val (Murrell-Lagnado and Aldrich, 1993b; Schott et al., 1998). It is

possible that the BP homologue used in our experiments may form a short α helix with an extended and highly charged COOH terminus (net charge, +6). The finding that this BP homologue readily blocks the DTX-bound form of the maxi-K_{Ca} channel is another strong piece of evidence that DTX-I itself does not bind within the internal conduction pathway or directly occlude the pore. Otherwise, the binding of DTX-I would be expected to completely prevent the binding of BP.

Binding of More Than One Kunitz Inhibitor per K_{Ca} Channel Tetramer Is Inhibited by a Structural or Electrostatic Mechanism

By the usual criteria, the solitary interaction of BPTI or DTX-I with single K_{Ca} channels behaves like a typical slow blocking reaction mediated by binding to a single class of sites, with the exception that a discrete substate, rather than a fully blocked state, is produced. These criteria include single-exponential dwell time histograms, an independent relationship between mean substate duration and peptide concentration, and a reciprocal relationship between the mean intersubstate dwell time and peptide concentration. Given that BPTI and DTX-I bind outside the central pore of a homotetrameric complex, this raises the question: why does the single-channel kinetics of these two molecules apparently conform to one-site behavior when each inhibitor is looked at alone?

Our work points to an answer that involves mutually antagonistic or repulsive ligand–ligand interactions. As presented in the RESULTS, we do find a state of mixed occupancy when these ligands are added together. The most compelling and direct evidence for this latter state is the lengthening of inter-DTX periods (τ_{BURST} in Fig. 4 B) as a function of BPTI. This measurement is a classic test for simple binding competition between two ligands at a common site. If there is only one site in common for both of the two ligands, τ_{BURST} should increase according to the term $\{1 + ([BPTI]/K_1)\}$, where K_1 equals the dissociation equilibrium constant of BPTI (Eq. 6). Instead, we find that τ_{BURST} is a much steeper function of [BPTI] than predicted by simple competition (Fig. 4 B). This "extra lengthening" can be explained by the existence of a doubly occupied $S_{BPTI/DTX}$ state. If DTX-I binds reversibly to a BPTI-occupied channel, the contribution of such events will result in extra lengthening of τ_{BURST} by the factor $(1 + [DTX]/J_2)$, where J_2 equals the equilibrium dissociation constant for DTX-I binding to the S_{BPTI} state (Eq. 7). An antagonistic binding interaction between BPTI and DTX-I is demonstrated by the finding that J_2 (178 nM) is 11-fold greater than the equilibrium constant for DTX-I binding alone (J_1 = 16.5 nM).

In our interpretation, the state of double occupancy by BPTI and DTX-I corresponds to short, nearly blocked (~1 s) dwell times within inter-DTX periods, since the frequency of these events is greatly increased in the presence of DTX-I plus BPTI, as compared with BPTI alone. However, these particular blocked events commence from a BPTI substate and virtually always end with a transition back to the BTPI-substate level. The fact that these events almost never terminate by a recognizable transition directly to the DTX sublevel implies that the order of binding of the two ligands is important. This suggests that a doubly occupied state reached by binding DTX-I as the last event is not structurally equivalent to one that is reached by binding BPTI as the last event. The explanation for this phenomenon is not obvious. It is possible that this behavior is due to structural changes of the channel protein that accompany the binding of these ligands. Complementary to these findings, there is also a significant lengthening of the apparent DTX substate as a function of BPTI concentration (Fig. 4 A). This behavior can also be accounted for by a state of double occupancy with an 11-fold lower affinity for BPTI in the S_{DTX} state vs. the unoccupied channel.

We can imagine two different types of mechanisms that would restrict the binding of more than one Kunitz inhibitor molecule to four presumably equivalent sites on a tetrameric channel complex. One possibility is that binding of one Kunitz molecule physically interferes with the binding of another Kunitz molecule. A precedent for this latter situation occurs in the crystal structure of human β tryptase (Barbosa Pereira et al., 1998). Tryptase is a serine proteinase from mast cells that forms a ring-like homotetrameric complex in which the four active sites face a central pore. This central pore on the β-tryptase tetramer is oval shaped with dimensions of roughly 30 × 50 Å. The geometry of this complex is such that the binding of only two molecules of an atypical Kazal-type proteinase inhibitor (leech-derived-tryptase-inhibitor, LDTI) to this complex is possible. Docking analysis indicates that it is only possible to simultaneously bind two LDTI molecules to two sites located on diagonally opposite corners of the tetrameric pore (Barbosa Pereira et al., 1998). This physical arrangement is analogous to the schematic representation of the $S_{BPTI/DTX}$ state shown in Fig. 4. This particular example of self-inhibition of ligand binding is also interesting with respect to our hypothesis that the COOH-terminal portion of *Slowpoke* K_{Ca} channels is homologous to the serine proteinase family (Moss et al., 1996a,b). If binding of BPTI and DTX-I is actually mediated by this COOH-terminal domain, then a tetrameric complex analogous to that formed by β tryptase could be the underlying structural basis of apparently antagonistic ligand–ligand interactions among Kunitz inhibitors.

Protein electrostatics provides another plausible explanation for a negatively coupled interaction. Both

BPTI and DTX-I have a large excess of positively charged residues with a net charge of +6 and +10, respectively (Fig. 1 A). If four equivalent binding sites on a tetrameric channel complex are arranged within close proximity, repulsive electrostatic forces could be responsible for inhibiting the binding of more than one protein ligand to these sites. The magnitude and direction of such repulsive forces would depend on the distance between the sites and the ionic strength, as well as the location and distribution of charged residues on the Kunitz inhibitors. At the ionic strength of these experiments (50 mM KCl), the Debye length is ~14 Å. Under these conditions, there could be significant through-space electrostatic interactions between Kunitz inhibitor proteins at distances up to 30 Å. The fact that states of double occupancy apparently occur more readily in the presence of a mixture of BPTI and DTX, in comparison to either inhibitor alone, could be due to the unique surface charge distribution of these two molecules (Lancelin et al., 1994) and the particular docking trajectories that they assume in the course of their respective binding reactions. Further experiments involving alterations of the charge distribution on Kunitz proteins and/or ionic strength will be required to test this electrostatic hypothesis.

Dendrotoxin Has a Locking Effect on the Binding of the Ball Peptide Homologue

The data of Figs. 5 B and 6 show that BP exhibits a high affinity blocking interaction with an equilibrium dissociation constant of $B_1 = 7.2$ nM. The single-exponential dwell time distribution of discrete BP-blocking events (Fig. 10 A) is consistent with a kinetically homogeneous site for BP located somewhere within the internal conduction pathway. The lifetime of this BP-blocked state has a mean value of 1.7 s in the absence of other peptide ligands (Fig. 6 A). DTX-I has a striking effect on BP-blocking kinetics. Comparison of Figs. 5 B and 7 shows that the average duration of BP-blocked states is dramatically lengthened in the presence of 460 nM DTX-I. Quantitatively, at this concentration of DTX, there is a 2.7-fold increase in the mean BP-blocked time (Fig. 8 A vs. 6 B). Intuitively, this implies that the binding of DTX-I must somehow stabilize the BP-blocked state of the K_{Ca} channel by slowing the rate of BP dissociation. This is exactly the opposite of what would normally be expected for an allosteric ligand–ligand interaction that is negatively coupled. If two ligands that bind to different sites exhibit mutual inhibition of binding at equilibrium, then each ligand would ordinarily be expected to enhance the dissociation rate of the other ligand. This unexpected subversion of a common kinetic assumption is perhaps the most interesting aspect of our results.

In essence, Fig. 8, Scheme 4B, is a classic model of a cyclic equilibrium describing two ligands binding to nonoverlapping sites on a protein. The only extra assumption is that the K_{Ca} channel is a homotetramer that can only bind one molecule of DTX-I at a time to four otherwise equivalent sites. Although this supposition invokes an extreme example of "negative cooperativity," it is supported by previous analysis of the kinetics of DTX-I-substate events and the negatively coupled interaction observed between DTX-I and BPTI discussed above.

While the biochemical literature contains many examples of ligand–ligand interactions described by cyclic models formally equivalent to Fig. 8, Scheme 4B, the present example of DTX-I and BP is one of the few cases (if not the only case) where all eight rate constants are experimentally accessible. The routes of analysis used to obtain values for the eight rate constants of Fig. 8, Scheme 4B, are briefly summarized in Table I. The rate constants b_1, b_{-1}, $4j_1$, and j_{-1} are directly measurable from the single-channel kinetics of BP and DTX-I alone. The rate constant, b_2, for association of BP to the DTX substate is measured directly from the shortening of the mean duration of the DTX substate as a function of BP concentration (Eq. 16 and Fig. 8 B). The value of the equilibrium constant, B_2, for BP binding to the DTX substate is obtained from titration of the probability of the unconditional BP-blocked state in the presence of DTX-I (Eq. 18 and Fig. 8 C). The dissociation rate constant b_{-2} is directly obtained from the known values of B_2 and b_2. The equilibrium constant J_3 for binding of DTX-I to the BP-blocked state is independently obtained from the unconditional mean dwell time of the BP-blocked state in the presence of DTX-I (Eq. 19 and Fig. 8 A). The rate constants $4j_3$ and j_{-3} can be extracted from the measured time constants of the biexponential distribution of BP-blocked dwell times (Eqs. 23 and 24, and Fig. 10 B). A similar, but more precise estimate of j_{-3} can be directly calculated from the relationship $j_{-3} = (J_3)(4j_3)$.

Mutual compatibility of the various measured parameters with Fig. 8, Scheme 4B, can be checked in three different ways: (a) the derived values of J_1, J_3, B_1, and B_2 satisfy the equilibrium relationship for microscopic reversibility (Eq. 20), (b) the derived rate and equilibrium parameters predict the measured conditional probabilities for entry into and exit from the BP-blocked state (Eqs. 21 and Eq. 22, and Fig. 9), (c) the measured rate constants satisfy the following kinetic microscopic reversibility relationship:

$$b_1 4j_3 b_{-2} j_{-1} = b_{-1} 4j_1 b_2 j_{-3}. \quad (25)$$

Eq. 25 is simply the well known thermodynamic rule that the product of rate constants for traveling around a reversible cycle in one direction must equal the same

product in the other direction (Colquhoun and Hawkes, 1995). Using the best estimates of Table I, the left side of Eq. 25 is equal to 2.74×10^{11} $s^{-4}M^{-2}$, and the right hand side is equal to 2.96×10^{11} $s^{-4}M^{-2}$. The discrepancy between these two values is only 8%, which is quite low considering the errors associated with the individual determinations. Thus, by at least three criteria, the system consisting of single K_{Ca} channels and two ligands (BP and DTX-I) is very well described by Fig. 8, Scheme 4B, with the values for all eight rate constants summarized in Table I.

Aside from the aesthetics of such calculations, it is pertinent to ask what new insights have been gained from this strenuous exercise in single-channel analysis. The essential revelations are summarized in Fig. 13. This cartoon illustrates how the kinetic results may be interpreted in the context of a plausible structural model of the BP/DTX-I interaction. The cartoon depicts the BP homologue as a pore blocker binding somewhere inside the internal ion conduction pathway. The Kunitz protein, DTX-I, is depicted as binding to an external site on one monomer that is close to, but not occluding, the pore entrance. Considering the likelihood of protein–protein electrostatic interactions discussed above, we propose that the unusual asymmetry in rate effects between the two ligands arises from the positioning of these ligands on a channel architecture. For example, one could imagine that the 44-fold decrease in association rate of BP binding to the DTX-occupied channel could be the result of a strong, transient repulsive interaction experienced by the positively charged BP molecule (net charge, +6) as it enters the pore by passing within close proximity to the positively charged DTX-I molecule (net charge, +10). If the BP molecule is located at some distance deep inside the inner mouth of the channel in its bound state, then DTX-I would not have to pass as close to BP in the course of its own association step and, thus, it would not experience a similar repulsive barrier to association with the channel. This asymmetry in the trajectories of the respective association and docking steps would then explain the smaller antagonistic effect for DTX association to the BP-occupied state (1.3-fold reduction) versus the 44-fold reduction in the association rate for BP binding to the DTX-occupied state.

Similar electrostatic considerations could also apply to the ligand dissociation reactions. If the BP-binding site is located some distance inside the pore, then BP may transiently experience strong electrostatic repulsion in passing by the bound DTX-I molecule as it attempts to dissociate from its site and return to the solution. Thus, the charged DTX-I molecule could create a local electrostatic barrier to BP dissociation at the mouth of the channel that would lower the effective BP dissociation rate constant and essentially act to lock BP inside the channel. In contrast, DTX bound to a site outside the pore would not be confined by such a local electrostatic barrier and its dissociation rate would simply be enhanced by the positively charged BP molecule located some distance inside the pore.

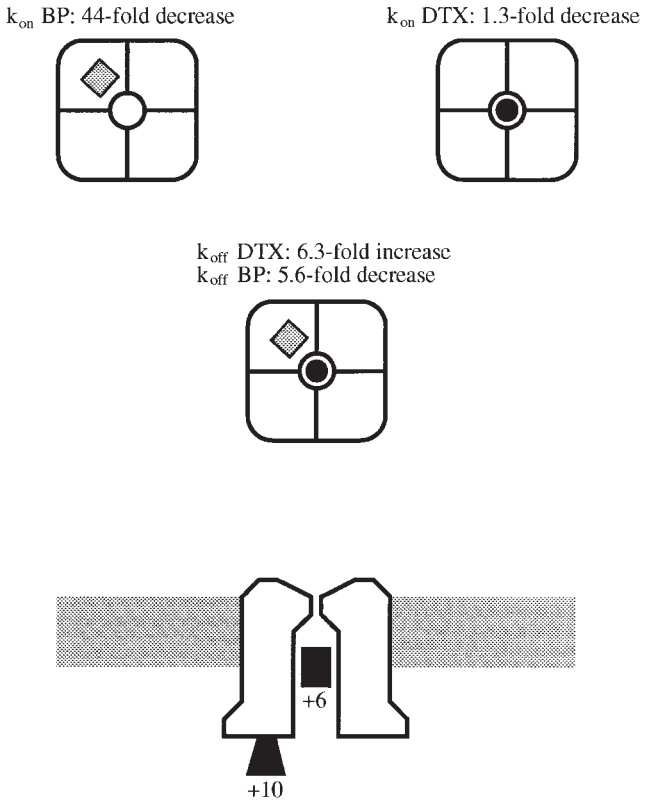

FIGURE 13. Cartoon drawing illustrating the changes in association and dissociation rate constants measured for the ligand interaction between DTX-I and BP on the internal side of the maxi-K_{Ca} channel. DTX-I is drawn as a diamond bound to one of the four K_{Ca} channel subunits and BP is drawn as the filled circle bound within the central pore. The top two drawings contrast the 44-fold decrease in the association rate constant of BP when DTX is bound as compared with a 1.3-fold decrease in the association rate of DTX-I when BP is bound. The middle drawing contrasts the opposite effects on the ligand dissociation rate constants of DTX-I and BP observed when the other ligand is bound. The lower drawing illustrates how a DTX-I molecule with a net charge of +10 could provide an electrostatic barrier to the entry and exit of BP with a net charge of +6.

Devising an unambiguous test of this electrostatic hypothesis is difficult, but such a model does make definite predictions for relatively simple experimental manipulations such as variation of ionic strength and decreasing the net charge of the ball peptide. It should also be noted that there is an alternative, but less parsimonious, explanation of the effects. One could argue that the observed rate effects are due to particular conformational changes in the structure of the channel protein induced by binding of the Kunitz peptides.

Since binding of DTX-I does induce some kind of rapid flickering of the open channel, which is the basis of the apparent subconductance events (Moss and Moczydlowski, 1996), it is possible that this effect contributes to observed changes in BP rate constants. However, it is not clear why such rapid conformational changes of the pore should not also be sensed by smaller and less charged blocking molecules, Ba^{2+} and TEA^{+}. The fact that these latter blockers of the internal conduction pathway do not exhibit a detectable ligand interaction with BPTI or DTX-I (Lucchesi and Moczydlowski, 1991) suggests to us that the electrostatic mechanism for the antagonism between DTX-I and BP is more likely to underlie this phenomenon.

Energetic Basis of a Negatively Coupled Ligand–Ligand Interaction

The theoretical basis of free energy changes associated with allosteric binding of two different ligands to two distinct sites on a protein molecule has been lucidly analyzed by Gregorio Weber (Weber, 1975, 1992). According to this formulation, cyclic reactions such as Fig. 8, Scheme 4B, are characterized by a coupling free energy, $\Delta\Delta G^0_{coup}$, defined as the standard free energy for binding a ligand X to a protein that already has another ligand Y bound, $\Delta G^0_X(Y)$, minus the standard free energy for binding the same ligand X to the unliganded protein, ΔG^0_X. Conservation of energy requires that the coupling free energies for the two possible pairs of binding energies are equivalent. For the two ligands of Fig. 8, Scheme 4B, these energy-coupling relationships may be expressed as:

$$\Delta G^0_{BP}(DTX) - \Delta G^0_{BP} = \Delta G^0_{DTX}(BP) - \Delta G_{DTX} = \Delta\Delta G^0_{coup}. \quad (26)$$

The standard free energy, ΔG^0, for a reversible ligand dissociation reaction with an equilibrium constant, K_d, is equal to $RT\ln K_d$, where R is the gas constant, T is absolute temperature, and K_d is the equilibrium dissociation constant. Using the respective values for K_d given as B_2, B_1, J_2, J_1 in Table I, the coupling free energy calculated for both the left and right hand side of Eq. 26 is equal to +1.3 kcal/mol. The absolute errors on these calculated free energies are ~0.1 kcal/mol. The fact that the two ways of calculating the coupling free energy in Eq. 26 yield identical results is simply a verification of microscopic reversibility discussed above. A positive value of coupling free energy corresponds to a negative or mutually destabilizing ligand–ligand interaction, whereas a negative coupling free energy corresponds to a positive or mutually stabilizing ligand–ligand interaction.

The value of +1.3 kcal/mol found for the antagonistic interaction between DTX-I and BP binding to the maxi-K_{Ca} channel falls within the range of ±2 kcal/mol typical of the magnitude of coupling free energies that have been previously measured for various ligand–ligand interactions on proteins (Weber, 1975, 1992). As noted above, our study is rather unique in that all eight rate constants for this ligand interaction have been experimentally determined. This allows us to analyze the relationships that govern the free energy coupling of the transition states for the various ligand-binding steps. The formal relationship between the equilibrium coupling free energy, $\Delta\Delta G^0_{coup}$, and the change in transition state energy for the respective dissociation and association reactions for BP and DTX-I can be readily derived by substituting the appropriate ratio of rate constants for the various standard free energies of Eq. 26 [e.g., $\Delta G^0_{BP} = RT\ln B_1 = RT\ln(b_{-1}/b_1)$]. Rearrangement of this substituted form of Eq. 26 leads to:

$$\Delta\Delta G^{\ddagger}_{diss}(BP) - \Delta\Delta G^{\ddagger}_{ass}(BP) = \Delta\Delta G^{\ddagger}_{diss}(DTX) - \Delta\Delta G^{\ddagger}_{ass}(DTX) = \Delta\Delta G^0_{coup}. \quad (27)$$

In Eq. 27, each of the respective changes for dissociation or association transition state energies, $\Delta\Delta G^{\ddagger}_{diss}$ or $\Delta\Delta G^{\ddagger}_{ass}$, is defined as the relative change in free energy for the respective reaction of a given ligand for the doubly occupied protein complex relative to the singly occupied complex. Thus, we have the following definitions:

$$\begin{aligned} \Delta\Delta G^{\ddagger}_{diss}(BP) &= RT\ln(b_{-2}/b_{-1}) \\ \Delta\Delta G^{\ddagger}_{ass}(BP) &= RT\ln(b_2/b_1) \\ \Delta\Delta G^{\ddagger}_{diss}(DTX) &= RT\ln(j_{-3}/j_{-1}) \\ \Delta\Delta G^{\ddagger}_{ass}(DTX) &= RT\ln(4j_3/4j_1). \end{aligned} \quad (28)$$

A positive value of the $\Delta\Delta G^{\ddagger}_{diss}$ means that the other ligand exerts an antagonistic (or repulsive) influence on dissociation rate of the reference ligand, whereas a negative value for this parameter means that the other ligand exerts a stabilizing influence and slows the dissociation rate of the reference ligand. Since a decrease in association rate constant is an antagonistic effect, the opposite interpretations apply to the sign of $\Delta\Delta G^{\ddagger}_{ass}$: a positive value is stabilizing, a negative value is destabilizing.

Fig. 14 depicts the respective change in transition state energies calculated from the rate constants of Table I in the form of a bar graph where the energies for the two ligands are plotted according to Eq. 27. This graph shows that the change in transition state energies for the two ligands appropriately subtract from each other to give a value very close to the equilibrium-coupling free energy of +1.3 kcal/mol, as expected from Eq. 27 and energy conservation. Fig. 14 also highlights the asymmetry in the change in transition state energies for the two ligands. DTX-I has a positive (destabilizing) change in transition state energy for dissocia-

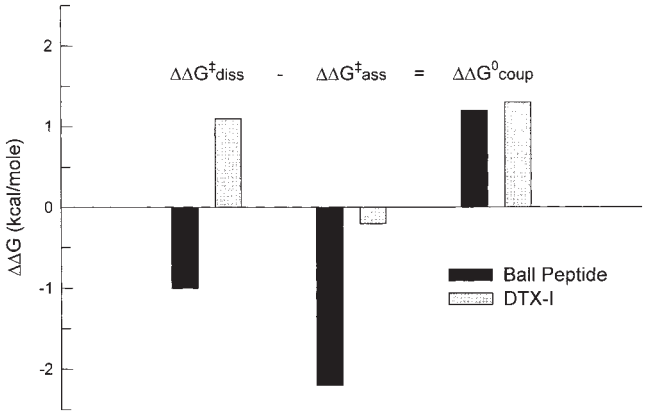

FIGURE 14. Relationship of free energy changes measured for the ligand interaction between DTX-I and BP. This energy diagram shows how asymmetric changes in the transition state energies for association and dissociation of two negatively coupled ligand-binding reactions can give the same equilibrium coupling free energy. The bar graph represents quantitative relationships described by Eqs. 26–28.

tion (+1.1 kcal/mol), whereas BP has a negative (stabilizing) value for this parameter (−1.1 kcal/mol). Both of the calculated changes in transition state energies for association are negative (destabilizing), but $\Delta\Delta G^{\ddagger}_{ass}$ for BP (−2.2 kcal/mol) is much stronger than that for DTX (−0.2 kcal/mol). As discussed above, these asymmetries in transition state energies provide important mechanistic insights. For purely electrostatic interactions, symmetrical effects between two ligands that bind in close proximity would be expected for situations where the binding trajectories essentially mirror each other on the protein surface. For a tetramer, such a situation would be expected for binding sites that lie in a plane of symmetry. The observation of highly asymmetric values for $\Delta\Delta G^{\ddagger}_{diss}$ and $\Delta\Delta G^{\ddagger}_{ass}$ in the present system is evidence for asymmetric pathways of ligand interaction such as that depicted in Fig. 13.

Summary

The molecular basis for apparent one-site binding kinetics of the positively charged Kunitz inhibitors, BPTI or DTX-I, to tetrameric maxi-K_{Ca} channels was explored by single-channel analysis of recordings carried out in the simultaneous presence of both ligands. Evidence was obtained for the existence of mixed states containing one DTX-I and one BPTI molecule simultaneously bound to the channel. Measurement of equilibrium binding affinity showed that bound DTX-I lowers the affinity for BPTI by 11-fold, and vice versa. Observations of the discrete block of the DTX-occupied channel by a potent BP homologue established that the binding site for DTX-I does not physically overlap with the site of internal entrance of BP to the pore. Analysis of single-channel records taken in the presence of DTX-I and BP revealed negative allosteric coupling between the binding of these two ligands to the K_{Ca} channel. In this interaction, the binding of one ligand decreases the equilibrium affinity of the other by eightfold, and vice versa. Mutually repulsive electrostatic interactions between basic peptide ligands binding within close proximity on the surface of a channel protein is a plausible explanation for the apparent negative cooperativity of ligand interactions between BPTI, DTX-I, and BP in this system. An interesting asymmetry in rate effects for the interaction between DTX-I and BP may be caused by an electrostatic barrier created by bound DTX-I at the channel's inner entryway that hinders both the association and dissociation reactions of BP.

This research was supported by a grant to E. Moczydlowski from the National Institutes of Health (GM-51172). I. Favre received support from a James Hudson Brown–Alexander Brown Coxe postdoctoral fellowship from Yale Medical School, an award from Novartis Stiftung, a postdoctoral fellowship from the American Heart Association (Connecticut Affiliate), and an award from the Swiss National Science Foundation.

Original version received 7 August 1998 and accepted version received 25 November 1998.

REFERENCES

Adelman, J.P., K.-Z. Shen, M.P. Kavanaugh, R.A. Warren, Y.-N. Wu, A. Lagrutta, C. Bond, and R.A. North. 1992. Calcium-activated potassium channels expressed from cloned complementary DNAs. *Neuron.* 9:209–216.

Anderson, C.S., R. MacKinnon, C. Smith, and C. Miller. 1988. Charybdotoxin inhibition of Ca^{2+}-activated K^+ channels. Effects of channel gating, voltage, and ionic strength. *J. Gen. Physiol.* 91: 317–333.

Atkinson, N.S., G.A. Robertson, and B. Ganetzky. 1991. A component of calcium-activated potassium channels encoded by the *Drosophila slo* locus. *Science.* 253:551–555.

Barbosa Pereira, P.J., A. Bergner, S. Macedo-Ribeiro, R. Huber, G. Matschiner, H. Fritz, C.P. Sommerhoff, and W. Bode. 1998. Human β-tryptase is a ring-like tetramer with active sites facing a central pore. *Nature.* 392:306–311.

Berndt, K.D., P. Güntert, and K. Wüthrich. 1993. Nuclear magnetic resonance solution structure of dendrotoxin K from the venom of *Dendroaspis polylepis polylepis. J. Mol. Biol.* 234:735–750.

Capasso, C., M. Rizzi, E. Menegatti, P. Ascenzi, and M. Bolognesi. 1997. Crystal structure of the bovine α-chymotrypsin:Kunitz inhibitor complex. An example of multiple protein:protein recognition sites. *J. Mol. Recognit.* 10:26–35.

Colquhoun, D., and A.G. Hawkes. 1995. The principles of the stochastic interpretation of ion-channel mechanisms. *In* Single Channel Recording. Plenum Publishing Corp., New York. 397–482.

Colquhoun, D., and F.J. Sigworth. 1983. Fitting and statistical analysis of single channel records. *In* Single Channel Recording. Plenum Publishing Corp., New York. 191–263.

Demo, S.D., and G. Yellen. 1991. The inactivation gate of the *Shaker* K^+ channel behaves like an open-channel blocker. *Neuron.* 7:743–753.

Doyle, D.A., J.M. Cabral, R.A. Pfuetzner, A. Kuo, J.M. Gulbis, S.L. Cohen, B.T. Chait, and R. MacKinnon. 1998. The structure of the potassium channel: molecular basis of K^+ conduction and selectivity. *Science.* 280:69–77.

Dufton, M.J. 1985. Proteinase inhibitors and dendrotoxins. *Eur. J. Biochem.* 153:647–654.

Favre, I., Y. Sun, and E. Moczydlowski. 1999. Reconstitution of native and cloned channels in planar bilayers. *Methods Enzymol.* 294: 287–304.

Foster, C.D., S. Chung, W.N. Zagotta, R.W. Aldrich, and I. Levitan. 1992. A peptide derived from the *Shaker* B K^+ channel produces short and long blocks of reconstituted Ca^{2+}-dependent K^+ channels. *Neuron.* 9:229–236.

Hollecker, M., D.L. Marshall, and A.L. Harvey. 1993. Structural features important for the biological activity of the potassium channel blocking dendrotoxins. *Br. J. Pharmacol.* 110:790–794.

Hoshi, T., W.N. Zagotta, and R.W. Aldrich. 1990. Biophysical and molecular mechanisms of *Shaker* potassium channel inactivation. *Science.* 250:533–538.

Kramer, R.H., E. Goulding, and S.A. Siegelbaum. 1994. Potassium channel inactivation peptide blocks cyclic nucleotide-gated channels by binding to the conserved pore domain. *Neuron.* 12:655–662.

Lancelin, J.-M., M.-F. Foray, M. Poncin, M. Hollecker, and D. Marion. 1994. Proteinase inhibitor homologues as potassium channel blockers. *Struct. Biol.* 1:246–250.

Latorre, R. 1994. Molecular workings of large conductance (maxi) Ca^{2+}-activated K^+ channels. *In* Handbook of Membrane Channels: Molecular and Cellular Physiology. Academic Press, San Diego, CA. 79–102.

Lucchesi, K., and E. Moczydlowski. 1990. Subconductance behavior in a maxi Ca^{2+}-activated K^+ channel induced by dendrotoxin-I. *Neuron.* 2:141–148.

Lucchesi, K.J., and E. Moczydlowski. 1991. On the interaction of bovine pancreatic trypsin inhibitor with maxi Ca^{2+}-activated K^+ channels. *J. Gen. Physiol.* 97:1295–1319.

MacKinnon, R., S.L. Cohen, A. Kuo, A. Lee, and B. Chait. 1998. Structural conservation in prokaryotic and eukaryotic potassium channels. *Science.* 280:106–109.

Meera, P., M. Wallner, M. Song, and L. Toro. 1997. Large conductance voltage- and calcium-dependent K^+ channel, a distinct member of voltage-dependent ion channels with seven N-terminal transmembrane segments (S0–S6), an extracellular N terminus, and an intracellular (S9–S10) C terminus. *Proc. Nat. Acad. Sci. USA.* 94:14066–14071.

Miller, C. 1995. The charybdotoxin family of K^+ channel-blocking peptides. *Neuron.* 15:5–10.

Miller, C., E. Moczydlowski, R. Latorre, and M. Phillips. 1985. Charybdotoxin, a high-affinity inhibitor of single Ca^{2+}-activated K^+ channels of mammalian skeletal muscle. *Nature.* 313:316–318.

Moczydlowski, E. 1992. Analysis of drug action at single-channel level. *Methods Enzymol.* 207:791–806.

Moss, G.W.J., J. Marshall, and E. Moczydlowski. 1996a. Hypothesis for a serine proteinase-like domain at the COOH terminus of *slowpoke* calcium-activated potassium channels. *J. Gen. Physiol.* 108:473–484.

Moss, G.W.J., J. Marshall, M. Morabito, J.R. Howe, and E. Moczydlowski. 1996b. An evolutionary conserved binding site for serine proteinase inhibitors in large conductance calcium-activated potassium channels. *Biochemistry.* 35:16024–16035.

Moss, G.W.J., and E. Moczydlowski. 1996. Rectifying conductance substates in a large conductance Ca^{2+}-activated K^+ channel: evidence for a fluctuating barrier mechanism. *J. Gen. Physiol.* 107:47–68.

Murrell-Lagnado, R.D., and R.W. Aldrich. 1993a. Energetics of *Shaker* K channels block by inactivation peptides. *J. Gen. Physiol.* 102:977–1003.

Murrell-Lagnado, R.D., and R.W. Aldrich. 1993b. Interactions of amino terminal domains of *Shaker* K channels with a pore blocking site studied with synthetic peptides. *J. Gen. Physiol.* 102:949–975.

Pietrobon, D., B. Prod'hom, and P. Hess. 1989. Interactions of protons with single open L-type calcium channels: pH dependence of proton-induced current fluctuations with Cs^+, K^+, and Na^+ as permeant ions. *J. Gen. Physiol.* 94:1–21.

Rettig, J., S.H. Heinemann, F. Wunder, C. Lorra, D.N. Parcej, J.O. Dolly, and O. Pongs. 1994. Inactivation properties of voltage-gated K^+ channels altered by presence of β-subunit. *Nature.* 369: 289–294.

Ruppersberg, J.P., R. Frank, O. Pongs, and M. Stocker. 1991. Cloned neuronal $I_K(A)$ channels reopen during recovery from inactivation. *Nature.* 353:657–660.

Schott, M.K., C. Antz, R. Frank, J.P. Ruppersperg, and H.R. Kalbitzer. 1998. Structure of the inactivating gate from the *Shaker* voltage gated K^+ channel analyzed by NMR spectroscopy. *Eur. Biophys. J.* 27:99–104.

Schreiber, M., and L. Salkoff. 1997. A novel calcium sensing domain in the BK channel. *Biophys. J.* 73:1355–1363.

Schweitz, H., C. Heurteaux, P. Bois, D. Moiner, G. Romey, and M. Lazdunski. 1994. Calcicludine, a venom peptide of the Kunitz-type protease inhibitor family, is a potent blocker of high-threshold Ca^{2+} channels with a high affinity for L-type channels in cerebellar granule neurons. *Proc. Nat. Acad. Sci. USA.* 91:878–882.

Shen, K.-Z., A. Lagrutta, N.W. Davies, N.B. Standen, J.P. Adelman, and R.A. North. 1994. Tetraethylammonium block of *Slowpoke* calcium-activated potassium channels expressed in *Xenopus* oocytes: evidence for tetrameric channel formation. *Pflügers Arch.* 426:440–445.

Sigworth, F.J., and S.M. Sine. 1987. Data transformations for improved display and fitting of single-channel dwell time histograms. *Biophys. J.* 52:1047–1054.

Skarzynski, T. 1992. Crystal structure of α-dendrotoxin from the green mamba venom and its comparison with the structure of bovine pancreatic trypsin inhibitor. *J. Mol. Biol.* 224:671–683.

Smith, L.A., P.F. Reid, F.C. Wang, D.N. Parcej, J.J. Schmidt, M.A. Olson, and J.O. Dolly. 1997. Site-directed mutagenesis of dendrotoxin K reveals amino acids critical for its interaction with neuronal K^+ channels. *Biochemistry.* 36:7690–7696.

Toro, L., M. Ottolia, E. Stefani, and R. Latorre. 1994. Structural determinants in the interaction of *Shaker* inactivating peptide and a Ca^{2+}-activated K^+ channel. *Biochemistry.* 33:7220–7228.

Toro, L., E. Stefani, and R. Latorre. 1992. Internal blockade of a Ca^{2+}-activated K^+ channel by *Shaker* B inactivating "ball" peptide. *Neuron.* 9:237–245.

Weber, G. 1975. Energetics of ligand binding to proteins. *Adv. Prot. Chem.* 29:1–83.

Weber, G. 1992. Protein Interactions. Chapman & Hall, New York. 293 pp.

Wei, A., C. Solaro, C. Lingle, and L. Salkoff. 1994. Calcium sensitivity of BK-type K_{Ca} channels determined by a separable domain. *Neuron.* 13:671–681.

Zagotta, W.N., T. Hoshi, and R.W. Aldrich. 1990. Restoration of inactivation in mutants of *Shaker* potassium channels by a peptide derived from ShB. *Science.* 250:568–571.